REPORT DOCUMENTATION PAGE

AFRL-SR-BL-TR-00-

0603

PLEASE DO NOT RETURN YOUR FORM TO THE ABOVE ADDRESS.

1. REPORT DATE (DD-MM-YYYY)	2. REPORT DATE	3. DATES COVERED (From - To)
31-10-2000	Final Technical Report	9/1/97 to 8/31/98

4. TITLE AND SUBTITLE
A Study of Phase Equilibria and Transformations in the Nb-Ti-Al System

5a. CONTRACT NUMBER
F49620-95-1-0116

5b. GRANT NUMBER
F49620-95-1-0116

5c. PROGRAM ELEMENT NUMBER

6. AUTHOR(S)
Vijay K. Vasudevan, N. Giridhar, B. Natarajan and K. Madangopal

5d. PROJECT NUMBER

5e. TASK NUMBER
2306/A5

5f. WORK UNIT NUMBER

7. PERFORMING ORGANIZATION NAME(S) AND ADDRESS(ES)
University of Cincinnati
Department of Materials Science & Engineering
Cincinnati, OH 45221-0012

8. PERFORMING ORGANIZATION REPORT NUMBER
AF-F49620-95-1-0116

9. SPONSORING/MONITORING AGENCY NAME(S) AND ADDRESS(ES)
Dr. Spencer Wu / Dr. Craig S. Hartley
Air Force Office of Scientific Research/NA
Metallic Strucural Materials,
801 N. Randolph Street,
Arlington, VA 22203-1977

10. SPONSOR/MONITOR'S ACRONYM(S)
AFOSR/NA

11. SPONSORING/MONITORING AGENCY REPORT NUMBER

12. DISTRIBUTION AVAILABILITY STATEMENT
Public

13. SUPPLEMENTARY NOTES

14. ABSTRACT

In this project, research effort was directed into phase equilibria and transformations in the Nb-Ti-Al system and in multicomponent gamma titanium aluminides. The sequence of transformations, site occupancies and stable phases in a 37Nb-37Ti-26Nb alloy were established, together with tie-lines at a number of temperatures between 1000-1300°C. The effect of beta-phase stabilizers, boron additions and thermal history on transformation pathways, modes, kinetics and microstructure in gamma Ti-Al alloys were established. Furthermore, isothermal and continuous cooling transformations for gamma alloys across a range of compostions from binary and ternary bases to multicomponent chemistries were studied. The reactions sequences for alpha and beta phases were quantified and partial CCT diagrams established for two multicomponent alloys. Mechanisms assocaited with various transformation modes are discussed.

15. SUBJECT TERMS
Phase equilibria; phase transformations; microstructure evolution; kinetics, mechanisms, Nb-Ti-Al system, TiAl alloys, alloying effects

16. SECURITY CLASSIFICATION OF:			17. LIMITATION OF ABSTRACT	18. NUMBER OF PAGES	19a. NAME OF RESPONSIBLE PERSON
a. REPORT	b. ABSTRACT	c. THIS PAGE			Vijay K. Vasudevan
U	U	U	UU	62	19b. TELEPONE NUMBER (Include area code) (513) 556-3103

A STUDY OF PHASE EQUILIBRIA AND TRANSFORMATIONS IN THE Nb-Ti-Al SYSTEM

Final Report

Work Performed Under

Grant No.: F49620-95-1-0116

Period: 9/1/97 to 8/31/98

Submitted By

Vijay K. Vasudevan, Principal Investigator
N. Giridhar, B. Natarajan and K. Madangopal

Dept. of Materials Science and Engineering, University of Cincinnati
Cincinnati, OH 45221-0012

To

Dr. Spencer Wu / Dr. Craig Hartley
Air Force Office of Scientific Research/NA
Metallic Structural Materials, 801 North Randolph Street
Arlington, VA 22203-1977

October 31, 2000

ACKNOWLEDGEMENTS

The principal investigator and supported postdoc and graduate students deeply appreciate the support provided by grant # F49620-95-1-0116 from the Air Force Office of Scientific Research, Dr. Spencer Wu, Program Monitor. The authors are also thankful to the Air Force Research Laboratory, WPAFB, Dayton, OH for providing the materials used in this work and for the use of various facilities (arc melting, heat treatments, DTA, chemical analysis). In addition, the authors wish to thank Dr. Dennis M. Dimiduk (AFRL) for colloborative work, helpful discussions and assistance, Dr. Robert Wheeler (UES) for his discussion and assistance in electron microscopy, Mr. Mark Dodd (UES) for help with some of the heat treatments, Mr. Tim Shock (UES) for help with the DTA runs and Mr. Tom Kerschner (UES) for the chemical analysis of the alloys. We also thank Dr. Pat Martin (now at UES) for providing some of the TiAl materials used in this study and for help in performing some of the heat treatments.

ABSTRACT

The work reported herein was performed by two M. S. students (N. Giridhar and B. Natarajan) and one postdoctoral research associate (Dr. K. Madangopal, 8/96 to 8/97) under the supervision of the P. I. Effort was directed in two areas: 1) Phase equilibria and transformations in the Nb-Ti-Al system and 2) Phase transformations and microstructure evolution in multicomponent gamma titanium alumindes. The work on the first was closely coordinated with the companion AFOSR AASERT project (award no. F49620-95-1-0487).

Phase equilibria and transfromations in a Nb-37Ti-26Al alloy were studied. The sequence of phase transformations in this alloy were established, together with tie lines at a number of temperatures between 1000 to 1300°C. The orthorhombic (O) phase was found to be the stable phase at temperatures <1000°C, with $\beta+\sigma$ being the stable phases between 1000 to 1325°C and only β above 1325°C. A composition invariant, displacive/martensite-like B2$\rightarrow$O transformation was observed. ALCHEMI results reveal that in the B2 phase (i) Al and Ti occupy two different, (ii) Nb partitions to both Al and Ti sites but prefers the Ti sites, and (iii) formation of Ti antisite occurs. On the other hand, in the O phase the Nb atoms tend to separate from Al and show a preference to occupy the Ti sites.

The effects of β-phase stabiliers and boron additions on phase transformations and microstructure evolution in Ti-47Al-2Cr-2Nb-1Mo-(0-0.2)B (in at.%) alloys were studied. The microstructures of the alloys in the as-cast, as-forged and heat treated conditions were characterized by optical, scanning and transmission electron microscopy. Analysis of the as-cast micro-structures of the alloys indicates that the solidification and solid-state transformation pathway was: L $\rightarrow$ L+β $\rightarrow$ α + β cores $\rightarrow$ lamellar ($\alpha+\gamma$) + β cores $\rightarrow$ lamellar ($\alpha_2+\gamma$) + B2 cores. In the alloys with boron, ribbon-like borides that have formed directly in the liquid are also present. The presence of the β phase and additions of boron are found to have complex, but somewhat different effects on transformations and microstructure development during cooling from the high temperature $\alpha+\beta$ or α regions. Boron has the dramatic effect of restricting α grain growth, of promoting the lamellar γ

morphology and lamellar growth rate and of suppressing the non-lamellar/feathery/massive γ mode of transformation. On the other hand, in the boron-free alloy, the feathery/ massive γ morphologies are favored over the lamellar morphology. In addition, the β phase forms as a thick continuous film along the prior α grain boundaries and is in association with several orientational variants of the γ phase. The β is found to be enriched in Cr and Mo and to transform to B2. With boron additions, the amount of the β/B2 phase reduces to where it is mainly present as particles enriched in Cr and Mo along prior α grain boundaries. In all cases the borides were determined to be TiB_2 and found to contain thin, interleaving layers of the B2 phase which have the following orientation relationship: (100) B2 // $(10\bar{1}0)$ TiB_2, [001]B2 // [0001] TiB_2. ALCHEMI results show that Al and Ti occupy different lattice sites in the B2 phase and that both Cr and Mo atoms have a strong preference for the Al sites. These results also seem to be borne out in the compostion determined for the B2 phase, which shows that the Ti concentration is ~50 at.% and the sum of Al, Cr and Mo roughly make-up the remaining 50%, with Nb probably distributed more on the Ti than Al sites. Based on the results obtained, the effects of the alloying additions on transformation pathways, modes, kinetics and microstructure are discussed.

Isothermal and continuous-cooling transformations for gamma alloys across a range of compositions from binary, and ternary bases to complex multicomponent chemistries of commercial interest were studied. Time-temperature-transformation curves are compared, and the effects of Al concentration and selected alloying additions (Cr. Mo, B) are highlighted. The reaction sequences for alpha-phase decomposition in gamma alloys was quantified. Special emphasis was placed on quantifying the heat transfer conditions used in the experimental study. The results lead to partial CCT diagrams for two multicomponent alloys that describe the temperature, time dependence of the various reaction modes.

Limiting reaction sequences in gamma alloys are massive gamma formation and cellular gamma formation at the highest and lowest cooling rates, respectively. Intermediate reaction products consist of $\gamma_L+\alpha$, $\gamma_W+\alpha$, and $\gamma_F+\alpha$, depending upon the alloy composition, cooling rate and grain size. The formation mechanisms and nature of the γ_W and γ_F microconstituents have been

proposed. Decompostion of the high temperature β phase is found to take two forms: precipitation of coarse γ within grain boundary films and as a cellular reaction leading to alternate γ and β lamellae. This reaction is driven by the reduced solubility of Al and increased Cr and Mo solubilities in the β phase with decreasing temperature. The β phase is found to have undergone ordering to a B2 structure, in which Ti atoms occupy one site, the Al, Cr and Mo atoms the other site and Nb partitioning about equally to both sites. Both the Al-level and the degree of transition-metal alloying can lead to marked (both favorable and unfavorable) shifts in the kinetic windows of formation of the various microconstituents. When such agents are used, the lamellar transformation kinetics may be significantly altered relative to other gamma alloys, thus changing the thermal process path and affecting the perfection of the lamellar microstructures. Reducing the Al-level and β-phase forming elements tends to mitigate unfavorable decomposition via cellular reactions.

TABLE OF CONTENTS

1. INTRODUCTION

There has been growing interest in intermetallic alloys for applications in high temperature, aerospace structural systems. Two broad classes of intermetallic systems have been studied: those based on the Nb-Ti-Al system, which are candidate materials for very high temperature (>1000°C) applications, and those based on γ-TiAl, which show great promise for use at intermediate temperatures (600-850°C). The properties of both classes of materials depend strongly on microstructure and hence on the phase transformations experienced during thermal processing. The objectives of the present program are two fold: 1) to study fundamental aspects of phase equilibria and transformations in the Nb-Ti-Al system, and 2) to study the effects of β phase stabilizers and boron additions on phase transformations and microstructure evolution in TiAl alloys.

2. SCOPE OF WORK

Research effort in this project has been directed in two areas. In the first, phase transformations and microstructure development in a 37Nb-37Ti-26Al alloy were studied with emphasis on a) establishing the low and high temperature phase equilibria, b) identification of decomposition pathways of the metastable and equilibrium phases, and c) determination of atomic site occupancy of elements in the B2 and O phases. This effort was closely coupled with the companion AASERT project (F49620-95-1-0487), results of which were described in detail recently [1]. In the second, multi-component TiAl alloys were studied with emphasis on determination of a) effects of beta phase stabilizers and boron additions on transformation pathways, microstructure evolution and transformation mechanisms, b) morphology of titanium borides, c) atomic site occupancy in the B2 phase and d) isothermal and continuous cooling reaction kinetics, microstuctural evolution and mechanisms of transformations. Materials and microstructure characterization was accomplished by differential thermal analysis (DTA), x-ray diffraction (XRD), optical (OM), scanning (SEM) and transmission electron microscopy (TEM), energy dispersive x-ray spectroscopy (EDS) in the TEM and electron probe microanalysis (EPMA). The technique of Atom Location by Chanelling

Enhanced Microanalysis (ALCHEMI) in the TEM was utilized in the determination of atomic site occupancies.

3. ACCOMPLISHMENTS

In the following, the results obtained and accomplishments made in each of the areas studied are described.

3.1. TRANSFORMATIONS IN THE 37NB-37TI-26AL ALLOY

This study was conducted by a graduate student, Mr. N. Giridhar, as part of his M.S. thesis and by a post-doctoral research associate, Dr. K. Madangopal. Related results on the overall Nb-Ti-Al system has been described in the final report of the companion AASERT project (F49620-95-1-0487 [1].

Experimental Details

The 37Nb-37Ti-26Al alloy was obtained as an arc-melted cigar (~125 mm long) from the Wright Laboratories, WPAFB in Dayton. The cigar was homogenized at 1600°C for 24h in vacuum followed by slow, furnace cooling. The transformation behavior was studied by DTA and heat treatment temperatures were selected based on these results. Cut samples of the homogenized alloy were reheated to 1400°C for 1h, water quenched, then aged at 700, 900, 1000, 1100, 1200 and 1300°C for times from 1 to 500h before quenching to room temperature. Materials and microstructure analysis was conducted by microhardness, OM, SEM, TEM, XRD, EPMA and fully quantitative EDS in the TEM. Pieces of the heat treated samples were crushed to powder for XRD determination of phases present, their structures and lattice parameters. The results obtained are described below.

Sequence of Transformations and Phase Equilibria

The β-transus for this alloy was determined to be near 1325°C. Samples quenched from 1400°C and above were single phase β (Figure 1(a)), but with evidence of weak B2 ordering

(Figure 1(b)). The microstructures of samples heat treated between 1000 to 1300°C were observed to be σ + B2 (formed from β at temperature on cooling), Figure 2. On the other hand, below 1000°C, the β phase transforms fully to the orthorhombic (O) phase, Figure 3, the latter appearing in a plate-like morphology consisting of multiple twin-related variants. The O phase was observed to be extremely fine in samples aged at 700°C. Furthermore, no other phases were observed even after long time aging to 500 hours. The sequence of transformations in this alloy can be summarized as follows:

1000-1325°C

$$\beta \rightarrow \beta + \sigma \rightarrow \text{on cooling} \rightarrow B2 + \sigma$$

<1000°C

$$\beta/B2 \rightarrow O$$

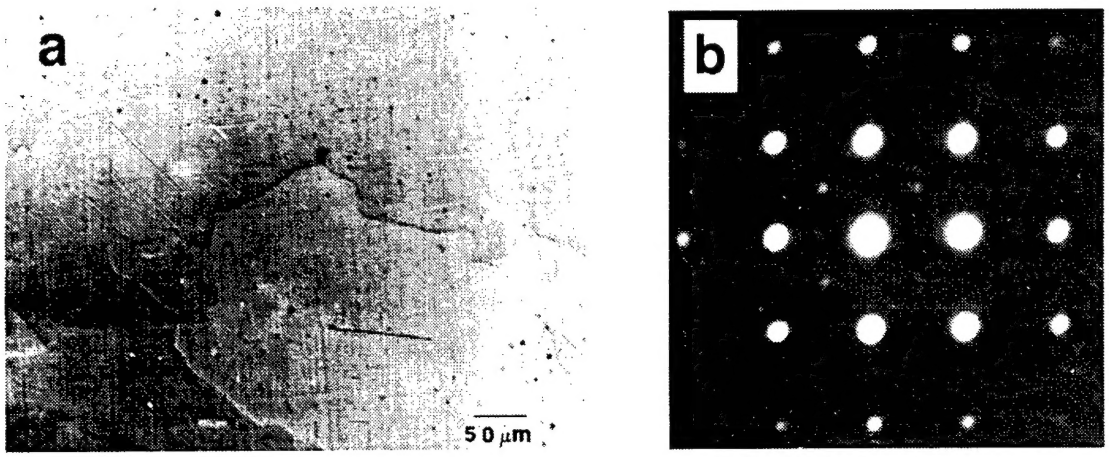

Figure 1. Microstructure of 37Nb-37Ti-26Al alloy water quenched after a hold at 1400°C, 1h. (a) OM showing single phase β microstructure; (b) [001] SAD pattern showing B2 superlattice reflections.

The phase chemistries at various temperatures (1000 to 1300°C) have been determined. These are shown in the ternary isothermal sections in Figure 4; the data of Perepezko *et. al.* [2] at 1200°C and 1100°C are also shown. As can be seen, the present results of the phase fields and the corresponding tie-lines at 1200 and 1100°C differ slightly with the results of Perepezko *et. al.* [2]

With a decrease in temperature over the range from 1300 to 1000°C, the σ phase composition can be seen to extend into the higher Nb side progressively. The β phase composition, on the other hand, increases into the Ti side of the phase diagram. This trend also results in the tie-line sweeping in the clock-wise direction from 1300°C to 1000°C. At temperatures <1000°C, only the O phase is observed, suggesting that it is the stable phase for this alloy at low temperatures. This is supported by the calculated ternary section at 700°C by Kattner *et. al.* [3],which shows a single O phase field close to the alloy composition of this study.

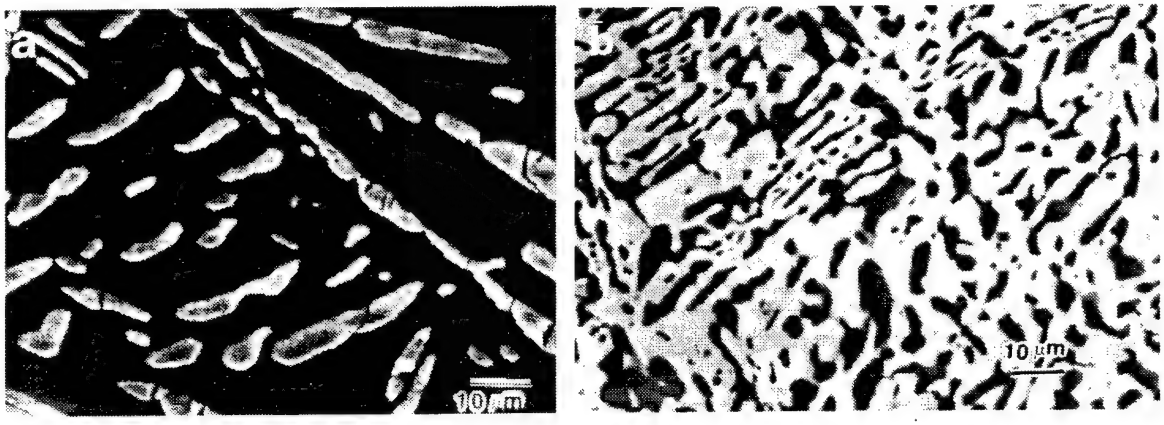

Figure 2. BSEI micrographs showing microstructure of solutionized (1400°C/1h/WQ) 37Nb-37Ti-26Al alloy aged at (a) 1300°C, 24h, WQ, and (b) 1100°C, 24h, WQ. (σ + B2).

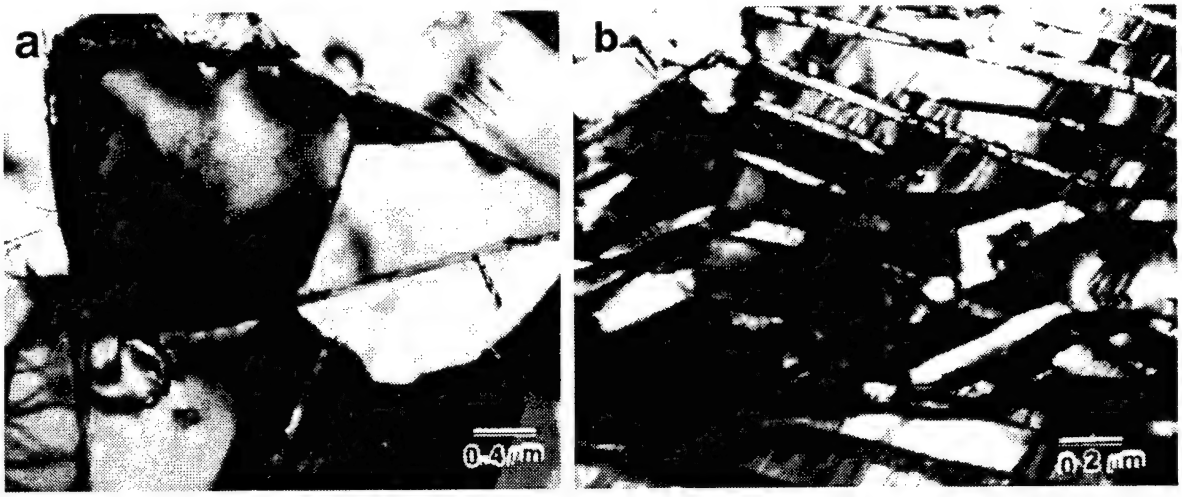

Figure 3. BF TEM micrographs showing microstructure of 37Nb-37Ti-26Al alloy solutionized at 1400°C,1 1h, WQ then aged at (a) 900°C, 1h, WQ and (b) 900°C, 200h, WQ. Fully O.

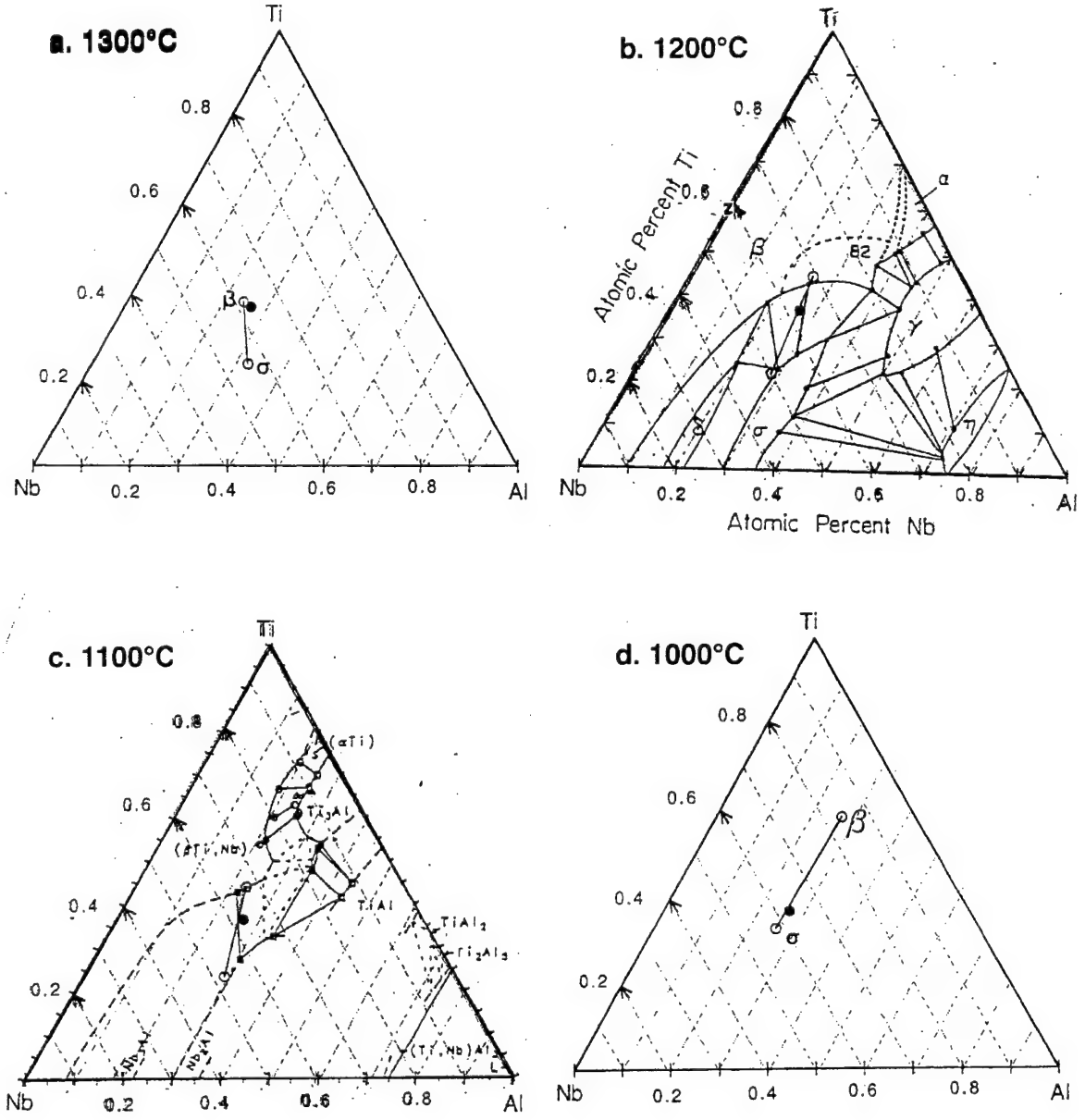

Figure 4. Tie-line data and phase chemistry in the Nb-37Ti-26Al alloy at (a) 1300°C (b) 1200°C (c) 1100°C and (d) 1000°C. Data of Perepezko et al. [1] is also included in (b) and (c).

B2→O Transformation

The transformation from B2 to O is quite fast, taking place within minutes at temperatures <1000°C. TEM observations (Figure 3) and electron diffraction established the O phase observed

herein to be similar to the orthorhombic Ti_2AlNb-type phase that has been previously reported in Ti-rich in Ti-Al-Nb aluminides [4-6]. The orientation relation between the two phases was also the same, being:

$$(011)\ B2\ //\ (001)\ O$$

$$[100]\ B2\ //\ [100]\ O$$

$$[\bar{1}\bar{1}1]\ B2\ //\ [110]\ O$$

EDS analysis in the TEM revealed that the B2 matrix (when present) and the O phase had nearly the same composition, both being near that of the overall bulk alloy composition. These observations suggest that the B2→O transformation is a composition-invariant, displacive/ martensite-like transformation, similar to the situation in the titanium-rich Ti-Al-Nb aluminides [5]. An orthorhombic phase has also been reported in a Nb-15Ti-15Al alloy upon isothermal aging of quenched material at low temperatures (i.e., 700°C) [7].

Further work is required to fully understand the nature of the B2→O transformation, i.e. whether it is shear, diffusional or a coupled mode. In the case of shear transformation, the site occupancies determined in the O phase should match those predicted from the site occupancies in the B2 lattice and the shear and shuffle involved in this transformation. In the case of the coupled transformation, one or two of the atom species would appear to form a rigid lattice, while the remaining diffuse between lattice sites.

Site Occupancy in the B2 and O Phases: ALCHEMI and Ordering Tie Line (OTL) Analyses

High resolution chemical analysis for determining the site preferences and site occupancies in the B2 and the O phases of Nb-Ti-Al alloys was performed using the ALCHEMI technique. The aim of this work is to shed light on the changes in site occupancies of Nb, Ti and Al during the B2 to O transformation, so as to ascertain the transformation mode.

General Strategy. ALCHEMI was performed under conditions of planar and axial channeling. The planar channeling condition is varied by setting the deviation vector, **s**, in a series

of positions of positive and negative deviation from the exact Bragg condition. The variation of x-ray yield under these circumstances reflects the variation of the relative magnitude of the fast electron flux at the alternate planes of the layered structure. Since these apparent compositions are the weighted average of the actual site compositions, the straight line passing through them on a ternary phase diagram, the ordering tie line (OTL), corresponds to the ratio of the Nb, Ti and Al atoms in these sites [8]. The actual site occupancy is then obtained from the OTL by determining the structure factor of the superlattice reflection.

In the present investigation, the Intersecting Kikuchi Line (IKL) technique has been selected to precisely determine the structure factors. In this technique, a three beam condition is set up where the Kikuchi line of the **g** vector under investigation intersects a relatively weak Kikuchi line of a high index reflection. The structure factor of the **g** vector is then derived from the extinction distance obtained as the inverse of the gap between the split segments of the weak Kikuchi line. However, in order to compute the accurate value of the structure factor, the dynamical interaction has to be taken into account. The general strategy using this technique is to compute the expected split distance as a function of site occupancy in different possible ordering scenarios using the dynamical theory of electron scattering and use it to obtain the scattering factor associated with the measured split distance. The site occupancies could alternately be determined from the difference in the x-ray yields in the maximum channeling condition and the non-channeling condition through simple equations which assume that at least one atom of the alloy is exclusively located on one of the sites. In the case of axial channeling too, the difference of the x-ray yields in the channeling and the non -channeling conditions is used to determine the site occupancies. In these channeling experiments, the actual compositions are obtained by correcting the apparent compositions using **k**-factors computed from the composition in the non-channeling condition, without the requirement to correct for absorption of x-rays. On the other hand, the x-ray yields during channeling is strongly affected by delocalization effects, which is particularly significant for characteristic x-ray energies below 4 Kev. In this investigation, multivariate statistical analysis will be applied to determine the correction factors for the delocalization effects.

In summary, the general strategy being employed in this study to determine the site occupancy is: (i) determining the OTL by ALCHEMI, after correcting for delocalization effects using multivariate analysis, (ii) determining the structure factor of the reflection used in channeling by the IKL technique, after correcting for **n**-beam dynamical interaction, and (iii) determining the actual site occupancy from the intersection of the OTL and the composition line corresponding to the structure factor. During this reporting period, task (i) above has been completed and the results obtained are described below.

Site Occupancy in the B2 Phase. Five samples containing the B2 phase were investigated in the ALCHEMI study. These consisted of a fully B2 sample obtained by quenching from 1400°C and four others containing B2 + σ phases obtained by subjecting the 1400°C, 1h homogenized alloy samples to aging treatments at 1300, 1200, 1100 and 1000°C for 200h. In the latter four samples, the compositions of the B2 and σ phases change with temperature, and this offers an avenue for studying the effect of chemistry of the B2 phase on site occupancy. The operating voltage of the TEM was set to 160kV so as to attenuate many-beam effects and a 20 μm diameter condenser aperture was employed to attain sufficient collimation of the electron beam. The specimens were tilted to orientations where a systematic row comprising of the 200 spots was excited in the B2 phase. Both planar channeling of the (100) and (110) planes and axial channeling in the [100] and [110] zone axes were performed. EDS spectra were then obtained as a function of the diffraction condition. Spectra were collected for each systematic row with the deviation from the Bragg condition, **s**, set to be negative and positive for the 100 spots, as illustrated by one example in Figure 5. The counts reported are within windows set to 1.2 FWHM (full-width half maximum) after subtraction of background and the hole counts. The count rates were adjusted to be approximately the same (~1800 CPS) for all the experiments.

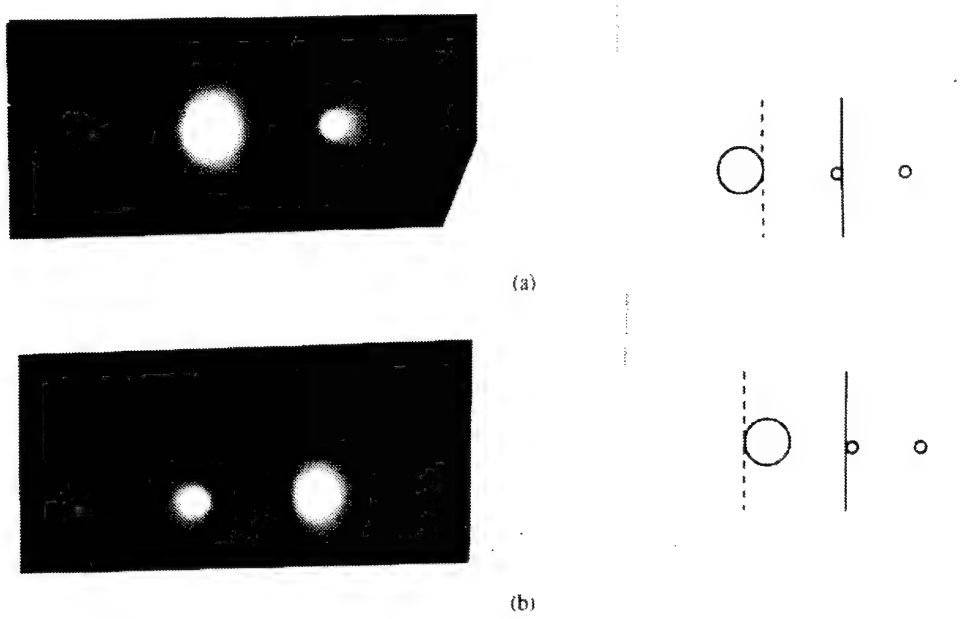

Figure 5. Diffraction patterns from the B2 phase showing conditions used in the ALCHEMI experiemtns. (a) s<0 (Kikuchi line inside the (100) reflection) and (b) s>0 (Kinuchi line outside the (100) reflection).

A thin foil from the sample quenched from 1400°C after holding for one hour and quenching was first analyzed. As this alloy was single phase B2, it was used as a standard for determining **k**-factors. The operating conditions that were employed were the same as those used for the ALCHEMI experiments described above. The regions of the foil from where spectra were acquired had thicknesses ranging from 1500-2000 Å. Figure 6 shows one representative foil thickness measurement routine.

The results from the channelling experiments are presented in Table 1. For performing an OTL analysis, the intensity data from the ALCHEMI experiments were converted to apparent compositions by using the **k**-factors, which were:

$$\mathbf{k}_{AlTi} = 1.655 \text{ and } \mathbf{k}_{TiNb} = 0.8414$$

The apparent compositions thus obtained are given in Table 2 and shown plotted in the ternary diagrams in Figure 7(a-d).

(a)

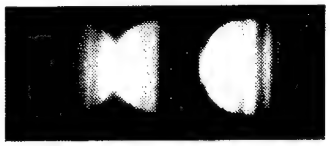

(b)

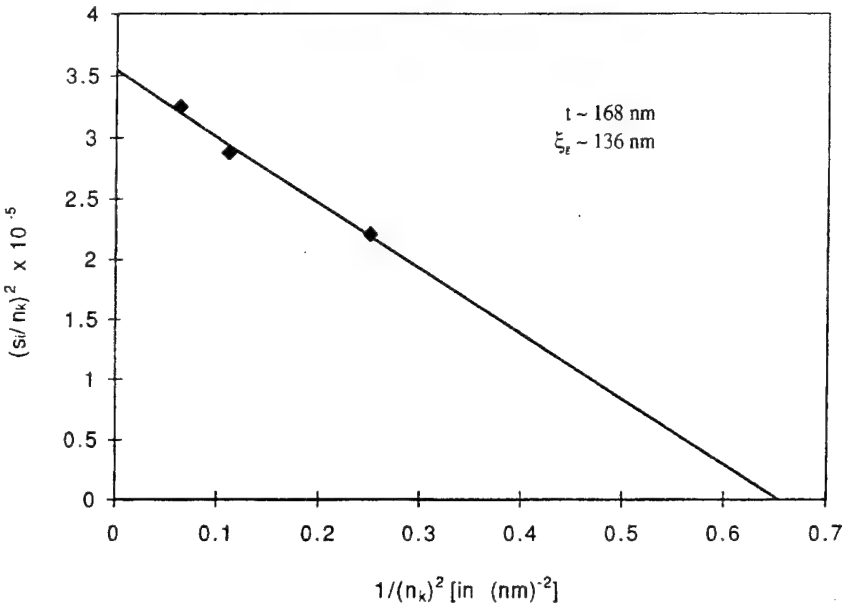

Figure 6. Kossel-Mollenstedt fringes in a ZOLZ CBED pattern from B2 phase in the Nb-37Ti-26Al alloy, quenched from 1200°C after a hold for 200h with (a) (110) strongly excited and (b) a plot of $(s_i/n_k)^2$ vs. $1/(n_k)^2$; intercept = $1/t^2$, Slope = $1/(\xi_g)^2$.

Table 1: Intensities from Channelling Experiments

Heat treatment	s	Al	Ti	Nb	Al/Ti	Nb/Ti	Al/Nb
1400WQ 1h + 1300WQ 200h	-ve	8392	22152	18353	0.379± 0.02	0.828± 0.025	0.457± 0.035
	+ve	7652	16377	14308	0.467± 0.027	0.873± 0.032	0.535± 0.042
1400WQ 1h + 1200WQ 200h	-ve	10702	36559	21158	0.293± 0.013	0.579± 0.025	0.506± 0.021
	+ve	11327	28331	17399	0.399± 0.018	0.614± 0.033	0.651± 0.025
1400WQ 1h + 1100WQ 200h	-ve	4543	17573	9626	0.258± 0.017	0.548± 0.035	0.472± 0.029
	+ve	4192	13036	7647	0.322± 0.0233	0.586± 0.044	0.548± 0.035
1400WQ 1h + 1000WQ 200h	-ve	6316	28713	16569	0.220± 0.012	0.577± 0.023	0.381± 0.023
	+ve	7815	24188	16667	0.323± 0.017	0.689± 0.027	0.469± 0.029

Table 2: Apparent Compositions Obtained from the Intensities and **k**-factors

Heat treatment	s	C^{app}(Al)	C^{app}(Ti)	C^{app}(Nb)
1400WQ 1h + 1300WQ 200h	-ve	27.50	48.10	36.9
	+ve	24.01	35.57	37.7
1400WQ 1h + 1200WQ 200h	-ve	27.67	41.81	30.5
	+ve	22.30	46.03	31.7
1400WQ 1h + 1100WQ 200h	-ve	23.87	44.86	31.3
	+ve	20.58	48.10	31.3
1400WQ 1h + 1000WQ 200h	-ve	17.76	48.78	33.5
	+ve	22.72	42.49	34.8

From Table 2 it is seen that changing the diffracting condition from $\mathbf{s}<0$ to $\mathbf{s}>0$ results in a significant relative increase in the Al/Ti ratios. The trends for the Al/Ti ratios are the same in all four samples investigated, namely, an increase in the ratios occurs on changing the diffraction condition from $\mathbf{s}<0$ to $\mathbf{s}>0$. This clearly implies that Al and Ti atoms occupy different sublattices. Henceforth, the α and β sublattices will be referred to as the Ti and Al sublattice. Furthermore, it is seen that when $\mathbf{s}>0$, the Al/Ti ratios are higher, therefore, sampling of the Al sublattice occurs in this condition.

It is also seen that a change from $\mathbf{s}<0$ to $\mathbf{s}>0$, results in an increase in the Al/Nb and Nb/Ti ratios, which implies that a majority of Nb atoms occupy the Ti sublattice. The trends are the same in all the samples, and so, the same deduction is made for all the cases.

Although the Nb/Ti ratios seem to increase on changing from the $\mathbf{s}<0$ to $\mathbf{s}>0$ condition, the variation falls within the error ranges and hence the ratios are taken as being constant. However, in the case of the sample aged at 1000°C, there is a significant relative increase in the Nb/Ti ratio. The constant Nb/Ti ratio gives rise to two cases: one in which all the Nb and Ti atoms occupy the same sublattice and the other in which Nb and Ti atoms are present in nearly the same ratios in both the sites. Stoichiometry does not allow for the first case and hence such a configuration is ruled out.

Therefore, the case of Nb and Ti atoms being present in both the sublattices is the most likely situation. In the sample aged at 1000°C, an increase in the Nb/Ti ratio indicates that the ratio of Nb atoms in the Ti sublattice to the Al sublattice is smaller than the ratio of Ti atoms in the Ti sublattice to the Al sublattice. Hence, the tendency of formation of Ti antisites is lesser in this case.

OTLs constructed for all of these cases (Figure 7(a-d)) intersect the Ti-Nb and Nb-Al side of the ternary diagram. This clearly suggests that Ti and Al atoms occupy different sublattices and supports the logical arguments that were presented above. Secondly, the OTL is extended to the Nb-Ti side of the phase diagram. The point where the OTL intersects the Nb-Ti side is designated as the composition of the Ti sublattice. From the composition obtained from the kinematic condition, the other end of the OTLs were determined. In all the cases it is seen that Nb atoms preferred the Ti sites. Figure 7(a) shows one such representative OTL construction. These results corroborate the above arguments and are obtained in a much simpler graphical representation.

In summary, the following points are made: (a) Al and Ti occupy two different sublattices in the B2 phase, (b) Nb partitions to both Al and Ti sites but prefers the Ti sites, and (c) formation of Ti antisite occurs. These results are in partial agreement with the work of Konitzer *et. al.* [9], who have reported that Nb atoms occupy Ti sublattice in the B2 phase in a Ti-24Al-11Nb alloy. However, in the present study it has been shown that Nb partitions into both Al and Ti sublattices. Lastly, the IKL method is being applied to determine the structure factor of the reflection employed in the ALCHEMI experiments in order to rigourously determine the end points of the OTL and thence the degree of long range order in the B2 phase as a function of chemistry.

Site Occupancy in the O Phase. ALCHEMI work was performed on the O phase in the 37Nb-37Ti-26Al alloy. Two types of samples were studied, one which had solutionized at 1400°C, followed by slow furnace cooling, and the second which had been solutionized at 1400°C, water quenched, then aged at 900°C. In the former case, the microstructure consisted of the O phase in a B2 matrix, whereas in the latter, it was fully O. Both planar channeling of the (200), (020), (220), (130) and (021) reflections and axial channeling in the [100], [010], [001] and [012] zone axes

were performed. CBED analysis of both slow cooled and aged orthorhombic structures have also been done. Preliminary analyses of the results show that in the O phase the Nb atoms show a tendency of separating from the Al sites, whereas in the B2 phase the Al and Ti separate to different sites while Nb partitions to both sites. The aim of the further analysis is to determine whether this site separation in the O phase is achieved purely by shear and shuffle or a combination of shear and shuffle.

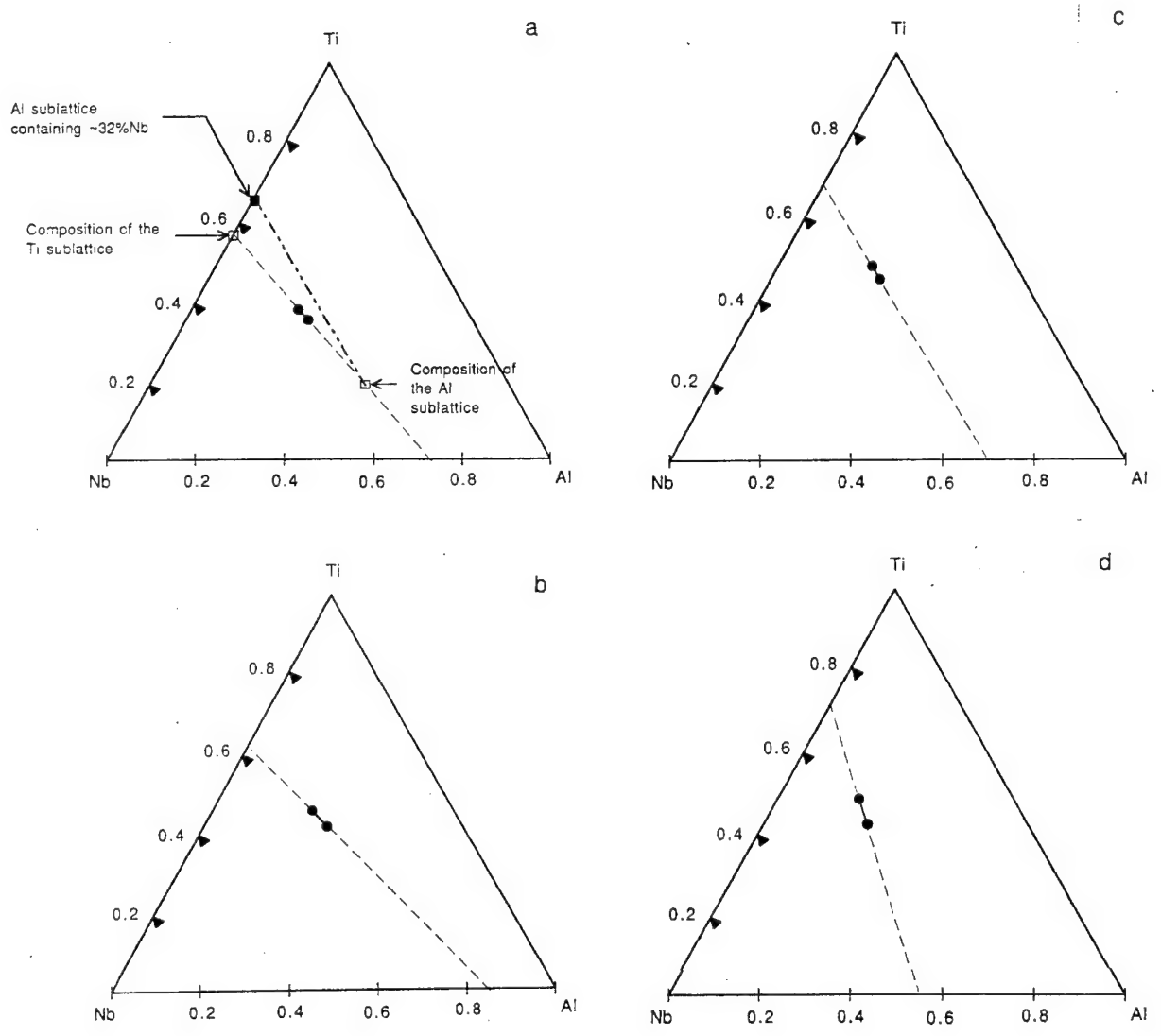

Figure 7. OTLs for the B2 phase in the Nb-37Ti-26Al alloy contained in samples heat-treated at (a) 1300°C (b) 1200°C (c) 1100°C, and (d) 1000°C.

3.2 TRANSFORMATIONS IN MULTICOMPONENT GAMMA TITANIUM ALUMINIDES

This work was conducted by another graduate student, Bharath Natarajan, as part of his M.S. thesis, and by a postdoctoral research associate, Dr. K. Madangopal (1996-97).

3.2.1 Effects of β-Phase Stabilizers and Boron Additions on Microstructure Evolution

The aim of this work is achieve a mechanistic understanding of the individual and combined effects of beta phase stabilizers and boron additions on microstructure evolution in multicomponent gamma titanium alumindes. The microstructures of Ti-47Al-2Cr-2Nb-1Mo-(0-0.2B) alloys in the cast, forged and heat treated conditions were characterized and the nature of the phases present, crystallographic relationships, and decomposition pathways studied.

Experimental Details

The chemical compositions of the five alloys which were studied in this work are presented in Table 3. While the four multicomponent alloys have almost the same overall composition, two of them additionally contain 0.2 at.% boron. Consequently, the microstructures of each set are expected to be similar in all conditions. Apart from these a binary Ti-48Al alloy containing 0.4B was also studied. Boron was added during alloy preparation in the form of AlB_2. The alloy ingots were processed by extrusion and double forging in one case, and only double forging in the other.

Table 3: Chemical Compositions of Alloys Studied.

Ingot Name	Composition (in at.%)
4. **Without Boron**	
Ti-25	Ti-47.5Al-1.8Cr-1.8Nb-1.0Mo (430 wt ppm Oxygen)
Ti-1126	Ti-46.6Al-1.8Cr-1.8Nb-0.9Mo (420 wt ppm Oxygen)
b. With Boron	
Ti-43	Ti-47.9Al-1.9Cr-1.8Nb-0.9Mo-0.2B (430 wt ppm Oxygen)
Ti-35	Ti-47.8Al-1.8Cr-1.8Nb-0.8Mo-0.2B (330 wt ppm Oxygen)
Ti-48Al	Ti-48Al-0.4B (nominal)

The forged ingots were subjected to intermediate recrystallization anneals at 1300°C for 2h between the forging steps and the final forging was conducted at 1100°C. Samples obtained from the hot worked ingots were heat treated at 1400°C and 1360°C for 1-2h and then either furnace-cooled (FC), air-cooled (AC) or water-quenched (WQ). The microstructures of the alloys in the as-cast, hot-worked and heat treated conditions were characterized by OM, BSEI-SEM, TEM, SAD and EDS; the latter three were conducted in a Philips CM20 200 kV TEM attached with an EDAX NX-2 ultra-thin window EDS system for chemical composition analysis of phases.

Results

In what follows, the two sets of the multicomponent alloys are referred to as those without boron and those with boron. Using resistivity measurements as a function of temperature [10], the α-transus, α-β transition and β-transus temperatures were determined to be near 1330, 1340 and >1420°C, respectively, for alloys with and without boron.

As-Cast, As-Forged Microstructures and Boride Morphology

The as-cast microstructure of the alloys without and with boron, Figure 8(a,b), is observed to consist of large fully lamellar grains (>500 μm), with evidence of a fine-scale structure within the grains. Under BSE imaging, Figure 8(c), a dendritic structure was clearly revealed, consisting of bright cores (the fine structure) surrounded by greyish regions and a dark network of the interdendritic regions. These observations suggest that the cores are depleted in Al and enriched in Ti, Cr, Nb and Mo and therefore possibly contain the β/B2 phase, whereas the interdendritic regions, where the last liquid solidifies, are enriched in Al, but depleted in the other elements. EDS spectra acquired from the center to the periphery of the dendrites essentially confirmed this. In the alloy with boron, Figure 8(b), thin ribbon-like structures, presumably borides, similar to those reported by others [11,12], were also present within the lamellar grains. TEM examination, Figure 9(a,b), established the microstructure in the dendrite cores to be composed of alternate bands of B2 and γ phases. The B2 showed the standard orientation relation with the γ associated with it in these regions and the surrounding α_2-γ lamellae, viz. $\{011\}B2 // \{0001\}\alpha_2 // \{111\}\gamma$ (Figure 9(b)).

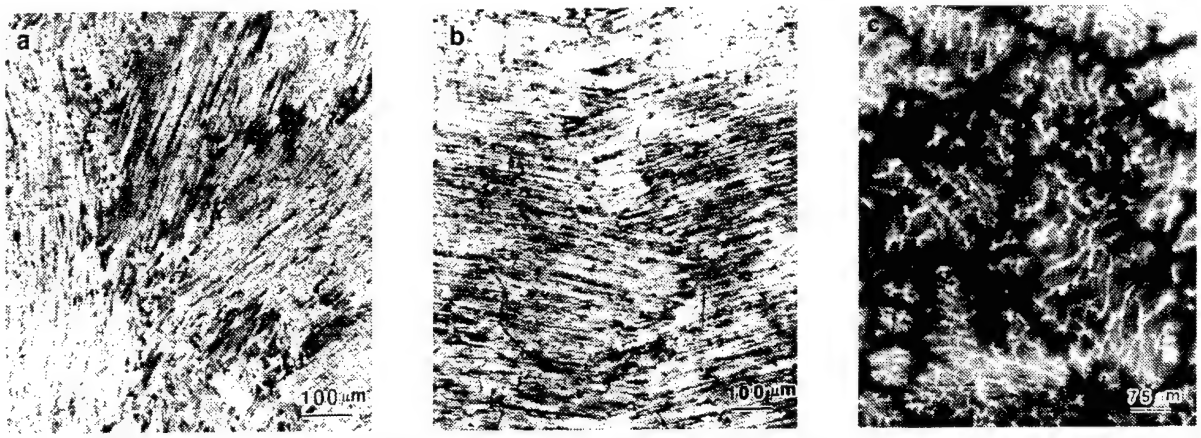

Figure 8. Micrographs showing as-cast microstructure of alloys. (a) 0.0B, OM; (b) 0.2B, OM; and (c) 0.2B, BSEI.

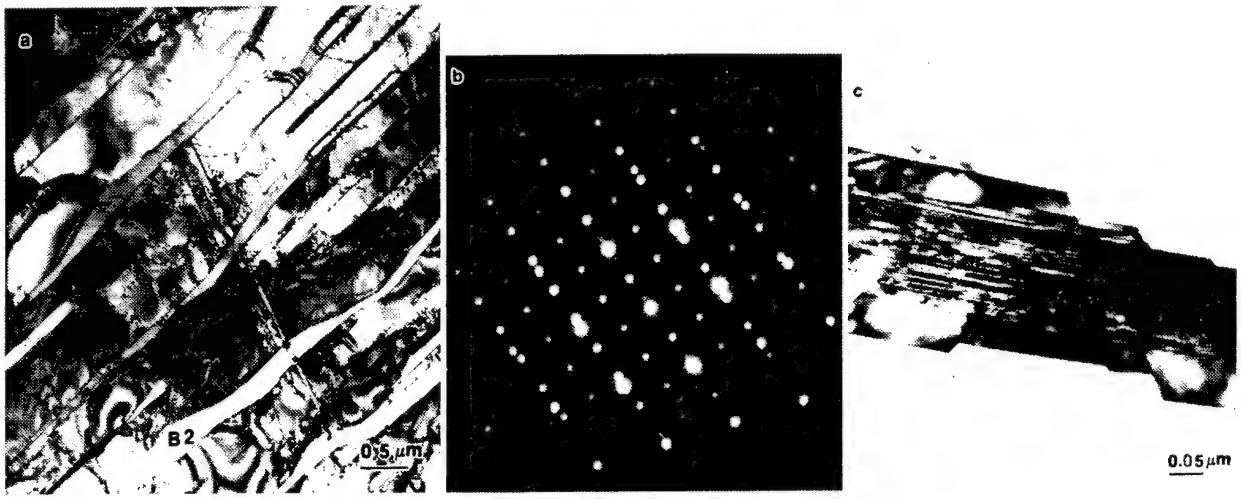

Figure 9. As-cast microstructure of 0.2B alloy. (a) TEM micrograph showing B2 cores with γ-α, lamellae; (b) [111] B2 // [011]γ // [11$\bar{2}$0]α, SAD pattern; and (c) TEM micrograph showing boride morphology.

It should be noted that there is a random distribution of the borides and the grain size looks unaffected, i.e. it is still large and comparable to the alloy without boron. This is related to the fact that the boride ribbons seem to be mostly located within the lamellar grains, i.e. in a random fashion throughout the microstructure cutting across primary dendrite arms and cored regions. Thus, it is conjectured that the boride ribbons in these alloys formed during the initial stages of solidification and were incorporated into the interdendritic regions between the growing β dendrites. Examination by SAD and TEM imaging, Figure 9(c), reveals the boride ribbons to possess a finely divided substructure composed of thin lamellae of TiB_2 interleaved with the B2 phase. The boride

ribbons appear to be much thinner in dimensions than those observed in other studies [11,12]. This may be due to the much lower amount of boron in the present alloys. The orientation relationship between the interleaving B2 and TiB_2 phases was determined to be: [010]B2 // $[1\bar{2}10]TiB_2$, (100)B2 // $(10\bar{1}0)TiB_2$. The habit plane or growth interface of the boride ribbons is found to be of the $\{10\bar{1}0\}TiB_2$ type, containing growth ledges of the $\{10\bar{1}0\}TiB_2$ type. It seems to follow from these observations that the ribbon-like morphology of the borides is essentially a result of its unique substructure and orientation relationship with the associated phase.

The microstructures of the alloys with and without boron in the as-forged condition appear, in the BSE micrographs, Figure 10(a,b), to be generally similar, consisting of small equiaxed γ grains and white particles at the grain boundaries. TEM and electron diffraction examination, Figure 10(c), revealed these particles to have the B2 structure (a_o = 0.316 nm) and to be predominantly present at the triple junctions of the γ grains. In the boron containing alloys, forging results in fragmentation of the boride ribbons into short lengths, which are found to be effective in pinning γ grain boundaries during subsequent heat treatments (Figure 10(d)). Presumably, these boride fragments, in association with the non-homogeneous concentration of plastic deformation in the surrounding regions, serve as sites for the nucleation of recrystallised γ grains. As before, the boride fragments were established to be TiB_2, with thin interleaving layers of the B2 phase present within them.

In order to clarify the role of beta stabilizers in the formation of the ribbon morphology of the borides, a binary Ti-48Al alloy without beta stabilizers, but containing 0.4B, was examined. In this alloy too, the TiB_2 borides were present in the ribbon morphology. TEM investigations reveal the substructure of these boride ribbons to be similar to those that occur in the alloys containing beta stabilizers, consisting of thin plates of TiB_2 interleaved with another phase. Though more work needs to be done to obtain incontrovertible evidence, there is substantial diffraction evidence to suggest that this phase is α_2. This is expected in Ti-Al alloys with high Al, where the α phase would be the phase to co-precipitate in the Al-rich regions adjacent to the TiB_2 laths. This

suggestion is supported by the observation of B2 as the interleaving phase in alloys containing beta stabilizers. The interleaved morphology of the borides in these alloys suggests an orientation relationship between TiB_2 and α_2. With the aim of unraveling the mechanism of formation of this morphology of borides in Ti-Al alloys with and without beta stabilizers, the following investigations are planned to be carried out : (i) characterization of the TiB_2 in TiAl alloys in terms of identifying the phases other than TiB_2 in the boride ribbons and determining the orientation relationships present between these phases using selected area and nanobeam diffraction and (ii) characterization of the substructural interfaces using high resolution TEM.

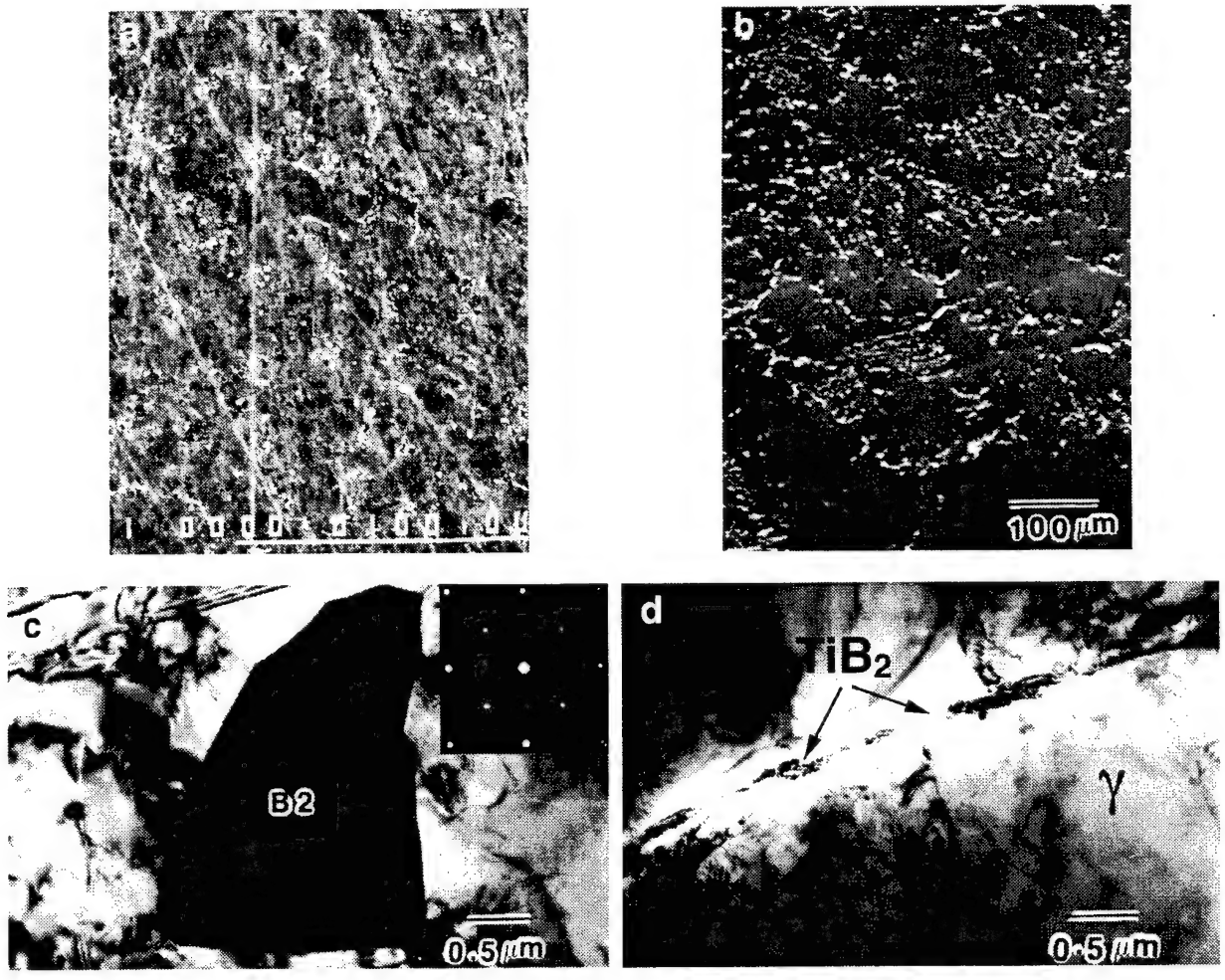

Figure 10. Microstructure of as-forged alloys. (a) 0.0B, BSEI; (b) 0.2B, BSEI; (c) 0.0B, TEM micrograph showing B2 particles with equiaxed γ grains (inset [001] B2 SAD pattern); and (d) 0.2B, TEM micrograph showing borides at γ grain boundaries.

Microstructures After Heat Treatment

The microstructures of the alloys with and without boron after heat treatment at 1360 or 1400°C ($\alpha+\beta$ phase field) for 1-2h followed by cooling are dramatically different. The microstructure of the boron-free alloy heat treated at 1360°C, Figure 11(a), is fairly coarse-grained with both lamellar and non-lamellar (massive/feathery) γ products and coarse and fine β/B2 particles (bright). In acute contrast, the boron containing alloy heat treated under the same conditions is fine- grained, fully lamellar, with a dispersion of fine, particles mostly along the prior α grain boundaries (Figure 11(b)). Additionally, α-grain growth appears to be significantly restricted in this alloy. The microstructure of the boron-free alloy air-cooled from 1400°C consists of a higher volume fraction of β/B2, which appears as almost-contiguous bright films in Figure 11(c), together with non-lamellar, feathery/massive γ (dark regions showing little or no contrast variations). The prior-α grain size is finer after this heat treatment compared with the one at 1360°C. Thus, the films of β that form at the higher temperature appear to be effective in restricting α grain growth, especially when continuous. TEM and electron diffraction examination of the same samples revealed that the thick layers of β at the grain boundaries have a B2 structure, and are associated with several different orientational variants of the γ phase (Figure 12(a)). Interestingly, two different crytallographic orientation relationships, namely: $(0\bar{1}1)$ B2 // $(\bar{1}11)$ γ, [111] B2 // [101] γ; and $(0\bar{1}1)$ B2 // $(\bar{1}11)\gamma$, [100] B2 // [101]γ // [110]γ, Figure 12(b-e), were seen to relate the γ and the B2 phases in these regions. These observations suggest that this γ has formed directly from the high-temperature β on cooling. Another observation is that the lamellae of the γ phase present in this region appear to be twin related orientation variants as seen from the SAD patterns in Figure 12(d-e).

The microstructure of the boron-containing alloy which was air-cooled from 1400°C appears practically similar to that cooled from 1360°C, i.e., it is fine-grained, fully lamellar and with the same dispersion of fine, bright particles along the prior α grain boundaries (Figure 11(d)). TEM examination of these samples revealed a near-lamellar structure with equiaxed γ grains in

between the lamellar grains and few particles of B2 at the γ grain boundaries (Figure 13(a)). Interestingly, the volume fraction of the B2 is much lower in this alloy as compared with the similarily heat treated boron-free alloy (Figure 12(a)). In addition, boride fragments were present, mostly at grain boundaries and on occasion at continuous intervals within the lamellar grains. As before, the borides, Figure 13(b),were established by SAD, Figure 13(c,d), to be TiB_2 and to contain a few intervening layers of B2 within them. The orientation relationship between the TiB_2, and B2 phases was determined to be as before: (100) B2 // $(10\bar{1}0)$ TiB_2, [001]B2 // [0001] TiB_2, Figure 13(c,d), which is the same as the one reported in previous studies [10,11]. EDS analysis indicated that in all cases— as-cast, forged and heat treated—Ti and B were the major components in the borides, with the other elements being present in very small amounts.

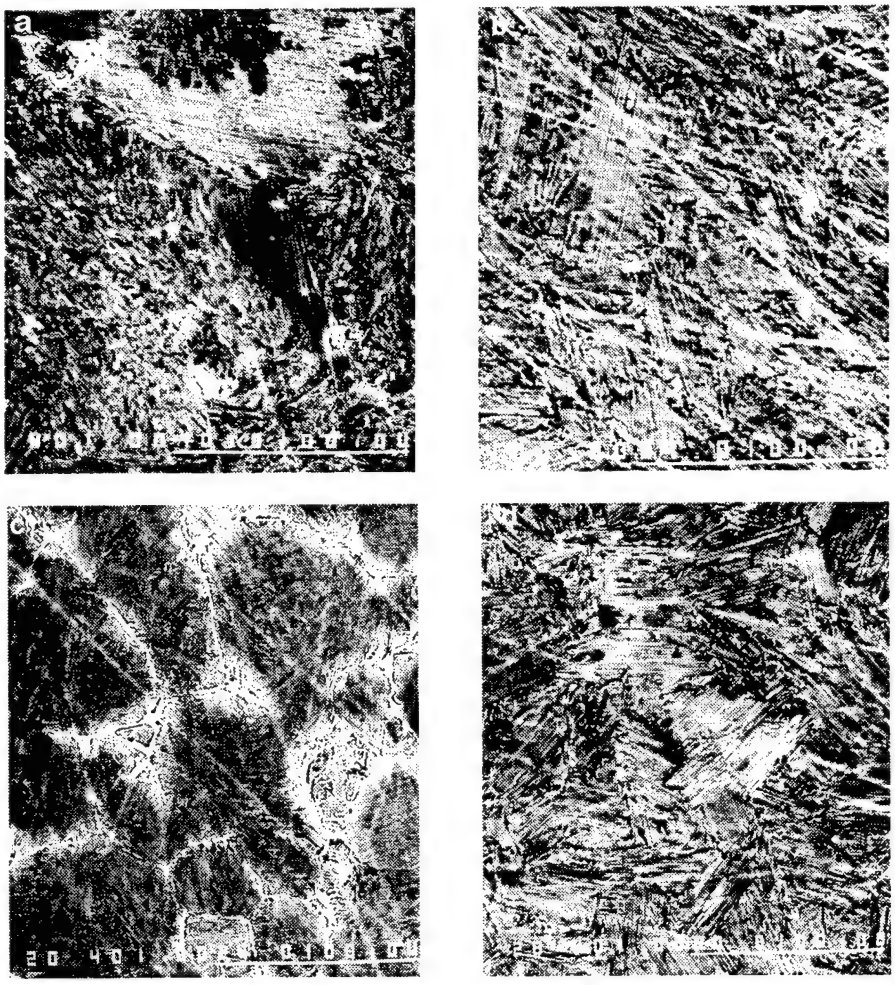

Figure 11. BSEI of 0.0B and 0.2B alloys, respectively, heat treated at 1360°C/2h/AC (a,b) and 1400°C/1h/AC (c,d).

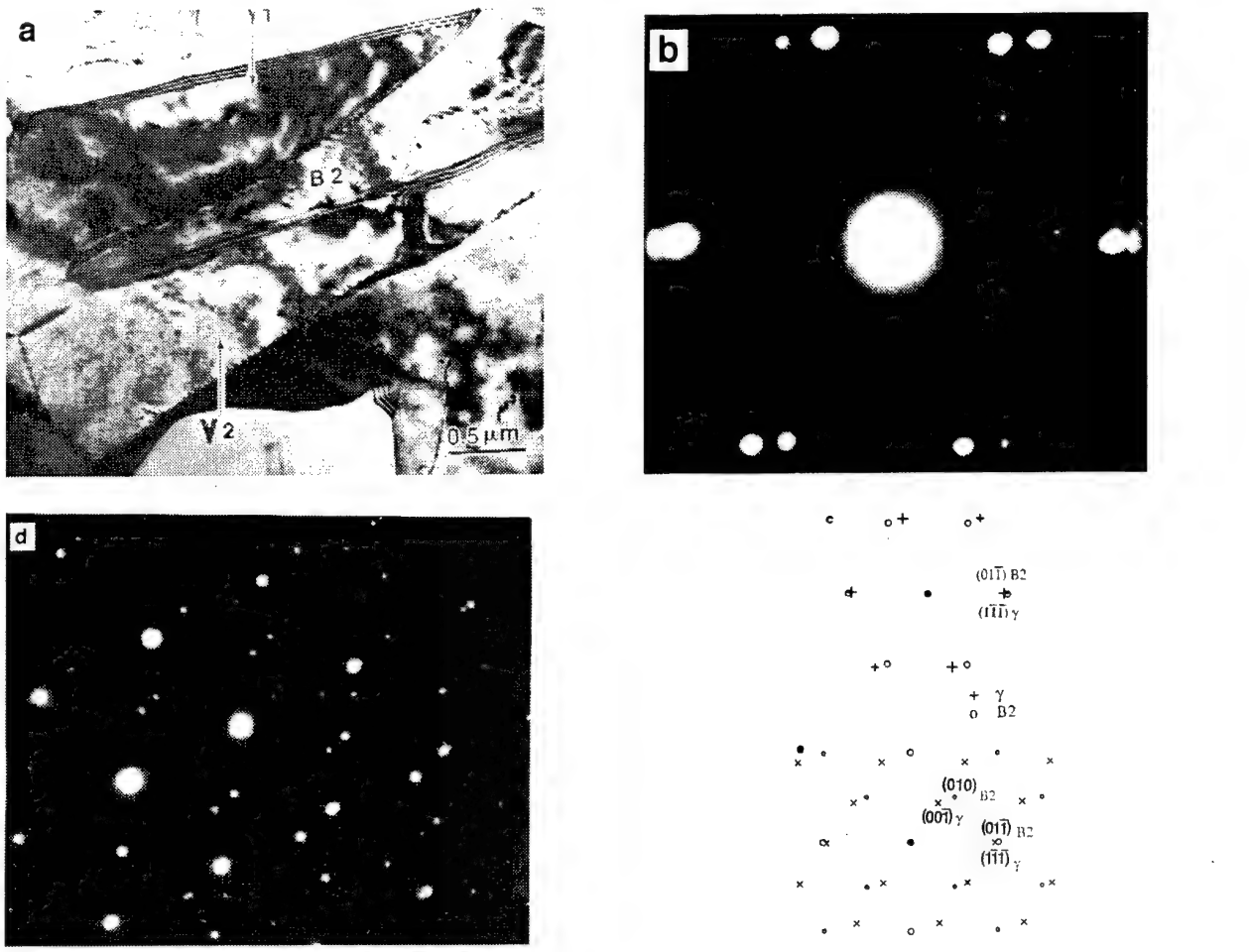

Figure 12. TEM micrographs of 0.0B alloy heat treated at 1400°C/2h/AC. (a) Grain boundary B2 films containing γ plates in several orientations; two orientation relationships between B2 and γ are depicted by (b,c) [111]B2 // [101]γ and (d,e) [100]B2 // [101]γ // [110]γ SAD patterns.

The lamellar γ morphology persisted in the boron-containing alloy even on water quenching from 1400°C, Figure 14(a,b), as compared with the boron-free material, which was a mixture of lamellar, feathery and massive γ (with B2 along the prior α grain boundaries), Figure 14(c,d). Furnace cooling from 1400°C lead to a fully lamellar structure in both boron-free and boron-bearing alloys, though the grain size of the latter was much finer and the lamellae somewhat coarser. In this case, the B2 phase in the boron-free alloy was present either as thin wavy structures or as triangular shaped particles at grain boundaries of large γ grains. As seen in the AC sample, these γ grains adjacent to B2 particles were also twin related. In Table 4, the results of EDS

analysis of the composition of the B2 phase in the different samples of the Ti-46.6Al-1.8Cr-1.8Nb-0.9Mo alloy are presented. As can be seen, in all cases the B2 phase is enriched in Cr and Mo to a greater extent and Nb to a lesser extent. However, the Cr and Mo enrichment is more pronounced in the as-forged and FC samples than in the AC or WQ samples.

TABLE 4: Composition (in at.%) of the B2 Phase in the Ti-46.6Al-1.8Cr-1.8Nb-0.9Mo Alloy

Condition	Ti	Al	Nb	Cr	Mo
As-forged	46.36	38.68	2.55	6.01	6.40
1400°C/1h/FC	49.46	33.36	2.45	8.26	6.46
1400°C/2h/AC	49.45	40.24	2.68	4.79	2.81
1400°C/1h/WQ	50.16	40.35	3.25	3.94	2.29

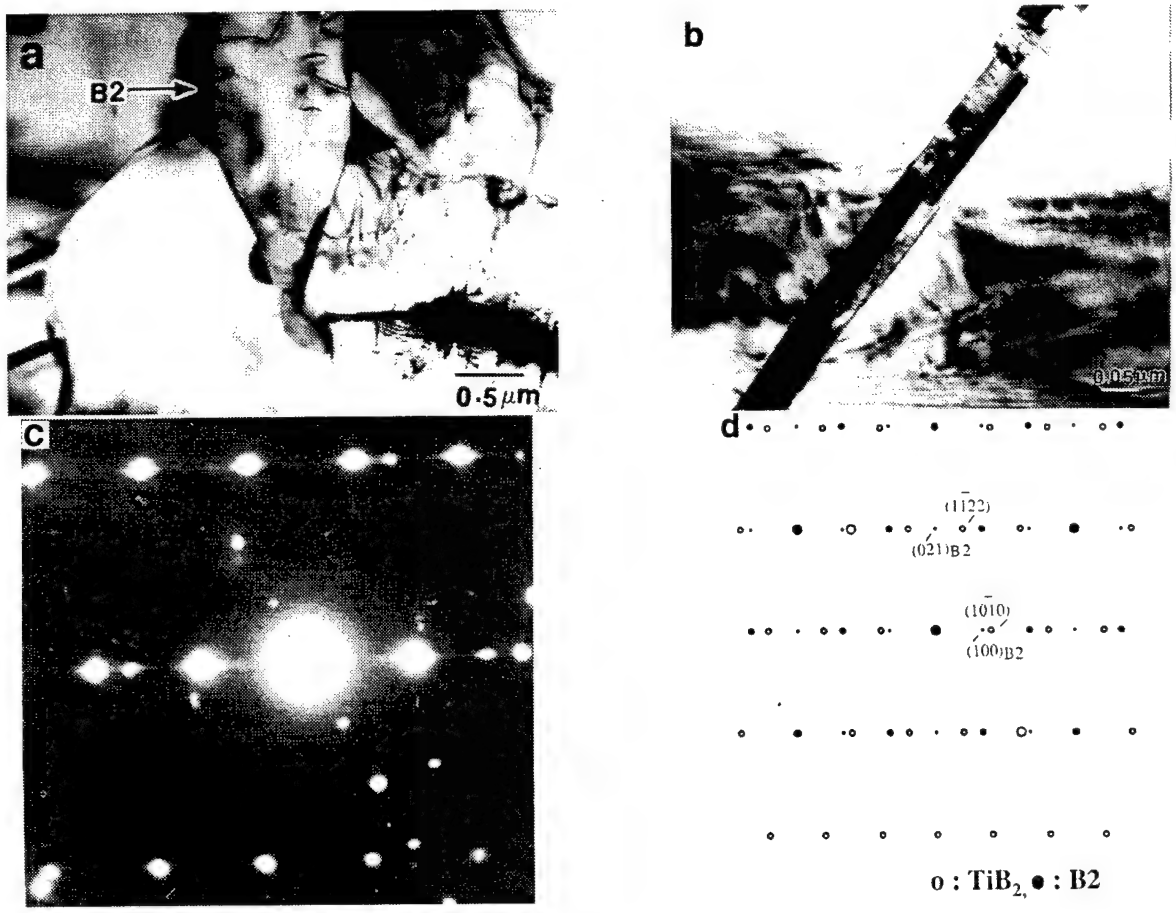

Figure 13. TEM micrographs of 0.2B alloy heat treated at 1400°C/2h/AC. (a) Grain boundary B2 particles; (b) a boride (TiB_2) plate containing thin layers of B2; (c) experimental; (d) simulated [2$\bar{4}$23]TiB_2 // [0$\bar{1}$2]B2 SAD pattern from composite boride plate in (b).

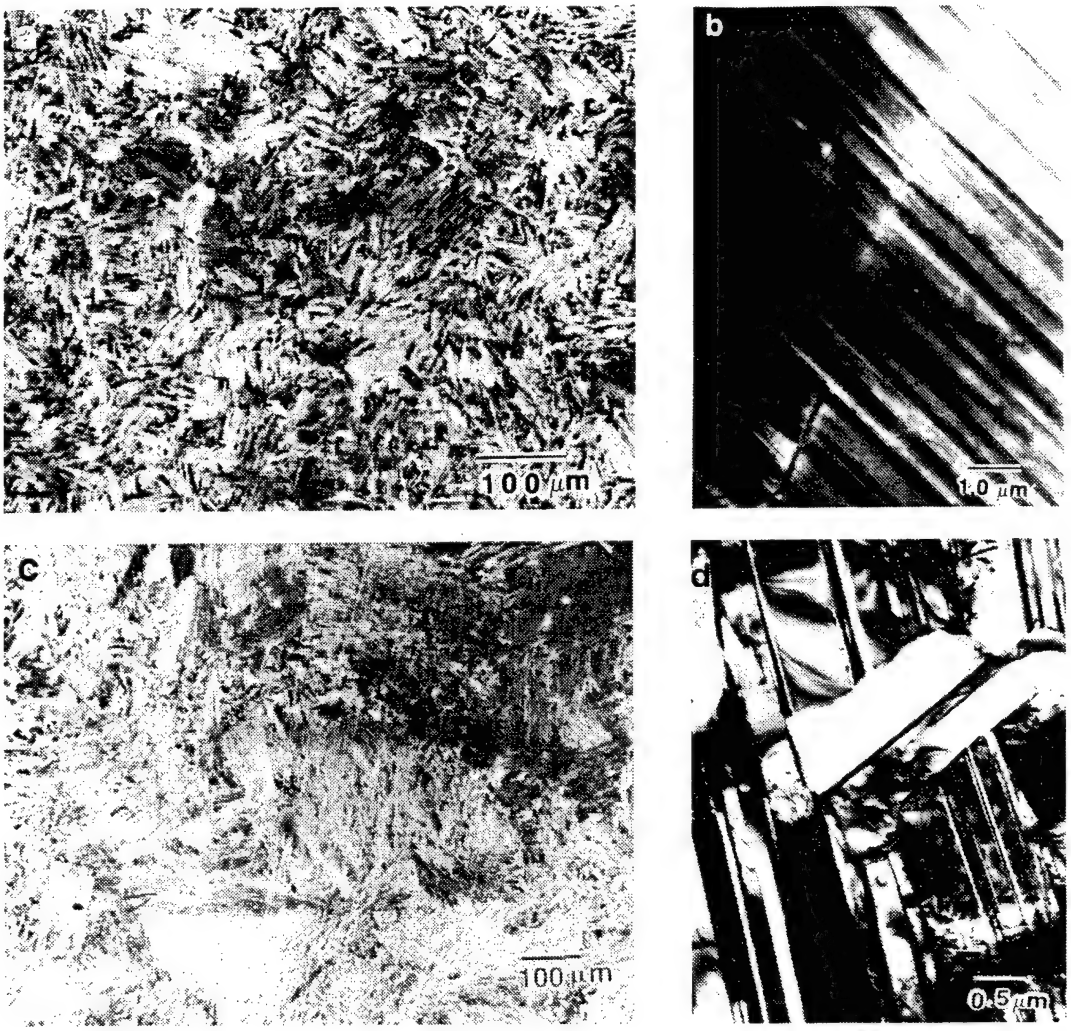

Figure 14. OM and TEM micrographs showing microstructure of 0.2B (a,b) and 0.0B (c,d) alloys heat treated at1400°C/0.5h/WQ.

Site Preferences in the B2 Phase

The site preferences of Cr and Mo atoms in the B2 phase present in the as-cast, forged and heat treated microstructures was investigated by ALCHEMI. Analysis of the results shows that Al and Ti occupy different lattice sites in the B2 phase and that both Cr and Mo atoms have a strong preference for the Al sites. The results of this work is to be documented for publication after the completion of analysis.

Discussion

The symmtery of the dendrite arms in the as-cast samples of the alloys with and without boron could not be clearly discerned in the present study, so that it is difficult to state definitively whether β or α is the primary solidification phase. However, a comparison of the microstructures of the cast samples with binary alloys of similar Al content [13] suggests that β is the primary solidification phase. This conclusion is the same as the one reached by Inkson *et al.* [11] in an Ti-45.5Al-1.6Fe-1.1V-0.7B alloy, but in contrast with that of Godfrey and Loretto [12] who studied Ti-47Al-2Cr-2Nb-(0.1-1)B alloys and proposed α to be the primary solidification phase. The observation of the B2 phase at the dendrite cores (Figures 8(c), 9(a)) further supports the idea that β is the primary solidification phase. The enrichment of Mo and Cr in the β phase promotes ordering of this phase to B2 at lower temperatures. The solidification and solid-state transformation pathway for the ensuing as-cast microstructure is deduced to be: L→L+β →α+β cores → lamellar (α + γ)+ β cores → lamellar (α_2 +γ)+B2 cores. However, since α_2/γ/B2 lamellae with a single orientation are observed, it is difficult to exclude the possibility that the L+β→α peritectic reaction above goes to completion and that the B2 phase is stabilized at lower temperatures in those regions of the α that were the cores of the prior β dendrites, or that a double peritectic reaction of the type L→L+β→L+β+α occurs, followed by transformation of the β cores to B2 and of α to the lamellar structure. More work is required to fully establish this. The occurrence of the borides mostly within the lamellar grains in the alloys with boron, and the ribbon-like morphology suggests that these borides have formed directly in the liquid, a conclusion also reached by Inkson *et al.* [11]. In agreement with their work, the borides are found to be TiB_2 interleaved with thin platelets of B2. The finely divided substructure appears to be a result of eutectic-like phase separation involving the co-precipitation of beta phase rich in Cr, Nb and Mo in regions adjacent to the TiB_2 phase or alternately an eutectoid like decomposition of a TiB precursor phase rich in beta stabilizers. It is imagined that formation of TiB_2 would result in the enrichment of the adjacent liquid layers with Cr, Mo and Nb, where the β phase would form.

The results presented have also shown that the presence of the β phase and boron additions have somewhat different effects on transformations and microstructure development during cooling from the high temperature α+β or α regions. Boron has the dramatic effect of restricting α grain growth, of promoting the lamellar γ morphology and of suppressing the non-lamellar, massive γ mode of transformation. On the other hand, in the boron-free alloys, the feathery/ massive γ morphologies are favored over the lamellar morphology.

The β phase in the boron-free alloys cooled from 1400°C (α+β phase field) occurs as thick layers at the grain boundaries of the α grains and becomes enriched in Cr and Mo, which, in turn, leads to the stabilization of the B2 phase at lower temperatures. In these alloys, α grain size is reduced only with a continuous or near-continuous layer of β around the grain boundaries. The β phase affects phase transformations only within it and the regions adjacent to. The occurrence of γ plates within the β/B2 regions with two different ORs suggests that these γ plates form directly from the β phase on cooling. The transformation behavior of the α grains around the β, on cooling, is similar to that of binary alloys of similar Al content [10,14,15], with the lamellar γ morphology dominating at low (FC) cooling rates and the feathery/massive and fully massive morphologies appearing in sequence at high (AC, WQ) cooling rates. However, lamellar γ nucleation appears to be inhibited by the presence of β phase. The lower volume fraction and particle-like distribution of the β/B2 phase in the alloys with boron is likely to be related to the smaller prior α grain size. The smaller the prior α grain size, the thinner the β films that form at the solutionizing temperature around the grain boundaries and the more complete it's transformation to γ on cooling.

The mechanisms by which boron additions bring about prior α grain refinement and promotion of the lamellar structure over the feathery and massive γ structures even on rapid cooling require consideration. At the level of 0.2 at.%B addition, there is little or no refinement of the as-cast grain size, but subsequent hot working and heat treatment do lead to considerable grain refinement. The evidence obtained to date in the present alloys, as well as those reported in other studies of similar alloys [11,12,16], indicates that all the added boron is present as TiB_2 primarily

and to a very limited extent in solid solution. This implies that there is probably no free boron available that might have segregated to the prior α grain boundaries and restricted their growth. On the other hand, in the forged material, and in those heat treated at high temperatures (1360-1400°C), TiB_2 particles were commonly observed at the γ-γ grain boundaries in the former and the lamellar grain boundaries in the latter. Thus, the refinement of the lamellar grain size is most likely due to the pinning of the prior α grain boundaries by the TiB_2 particles. The plate-like shape of these particles is probably quite effective in exerting strong restraining forces against grain boundary migration, so that very few particles need be present along the grain boundaries. However, the presence of some TiB_2 particles within the lamellar grains in heat treated specimens, in contrast with the situation in forged specimens, where they are located entirely at the grain boundaries, suggests that in some cases the grain boundaries are able to unpin and migrate. Other factors that are probably influential in restricting grain growth are the layers of γ grains that are often observed to be present at the lamellar grain boundaries, together with small β/B2 particles at the γ-γ grain boundaries. More work is required to ascertain whether these constituents play a significant role in α grain growth and the subsequent transformations.

Perhaps the most intriguing effect of boron is the promotion of the lamellar γ structure over the feathery and massive morphologies, even at high cooling rates, unlike the situation observed in the boron-free alloys, as well as in binary alloys of similar Al content [10,14,15]. One might speculate that this change is related to the refinement of the prior α grain size brought about by the TiB_2 particles. In this regard, the finer grain size may be expected to enhance the nucleation frequency of the lamellar γ in α, such that this transformation can begin at smaller undercoolings and go to completion before the samples have cooled sufficiently below the α/γ T_o temperature, where the driving force for the massive transformation becomes substantial enough for this morphology to appear. More experimental work on the determination of the reaction kinetics and temperature dependence (i.e, start and finish temperatures) of the different modes of transformation, has been performed on selected alloys and the results are described in the following section.

3.2.2 Isothermal and Continuous Cooling Kinetics, Microstructure Evolution and Mechanisms

In this section of the work, past literature is reexamined and the results of new experiments are reported, describing the kinetics of α and β-phase decomposition in gamma aloys. The time-temperature-transformation (TTT) or continuous-cooling-transformation curves for binary, Cr-containing ternary, and selected multicomponent gamm alloys are compared. The results are examined in an effort to qualitatively describe the influences of alloying on obtaining particular microconstituents. Emphasis is placed on producing fully-lamellar microstructures, since this alloy form is known to have the best combination of high-temperature properties and fracture resistance in the gamma alloy class [17]. This work was performed in collaboration with Dr. Dennis Dimiduk of AFRL, Dayton. The heat treatments described were performed either using the facilities at AFRL or those at the Rockwell Science Center. TEM facilities at AFRL were also utilized.

Experimental Procedures

The primary alloys used in this part of the work, whose analyzed chemical compositions are given below in Table 4, were produced using the following processes: *(1) Alloy "45-2-2."* This material was initially induction-skull melted and poured into a 70 mm dia. Mold at FlowServe Co. (Dayton, IH). The ingot was sectioned into billets, which were subsequently forged into round plates having a thickness of ~14 mm after a total plastic strain of 70% at Wyman Gordon (Houston, TX). A forged plate was given a recrystallization heat treatment in vacuum at 1215°C for 8 hrs. followed by furnace cooling. Square-rod-like sections having a cross-section of 14x12 mm, and variable lengths greater that ~50 mm, were used for all subsequently-described heat treatments. The α-transus tempeatue (T_α) for thismaterial was measured to be 1295°C. *(2) "Alloy 47-2-2-1."* This alloy was plasma-arc melted (PAM) and continuously cast into a ~350 mm dia. mold. The ingot was extruded, sectioned, and isothermally forged at Wyman Gordon, and supplied as 30 mm x ~400 mm dia. plate. Small cube-like sections having nominal dimensions of 12 x 12 x 12 mm were prepared for heat-treatment studies. This alloy had a measured T_α of 1345°C. Heat-treatment

results of these alloys are compared directly with those of binary and ternary materials reported in other studies [18-21], as well as with those of the multicomponent alloys reported in section 3.2.1.

An essential aspect of this study was to control cooling rates and isothermal exposure times during heat treatment. To accomplish this, cooling-rate estimates were made for the sample geometries used, based upon various literature data for gamma alloys compiled by Semiatin *et al.* [22]. In selected instances, these estimates were checked using heat-transfer analysis tools, contained in the commercial software "DEFORM," and by monitoring the cooling rates directly using instrumented samples. Having such estimates, samples were heat-treated in air and hot salt, without any surface treatments or protectic coatings. Continuous furnace cooling (FC) rates were accomplished in programmable air furnaces of comparable or larger thermal mass as the specimens, or by air cooling (AC). Near-isothermal treatments were accomplished both by rapid (<2 sec) transfers between preset furnaces (FQ), or by quenching into a liquid salt pot maintained at the specified temperature (SPQ). The latter treatments were performed at Rockwell.

Table 5: Chemical Compositions of Alloys Studied.

Ingot Name	Composition (in at.%)
994 or Ti-45-2-2	Ti-45.3Al-2.1Cr-2.0Nb (610 wt ppm Oxygen)
3-95 or Ti-47-2-2-1	Ti-46.5Al-2Cr-2Nb-0.9Mo-0.2B (400 wt ppm Oxygen)

Results and Discussion

In the following, the results of the reaction starts, modes, microstructure evolution, transformation mechanisms and comparisons with binary, ternary and other multicomponent alloys are described.

Reaction Start Estimates

Figure 15 shows the estimated transformation start temperatures and times during continuous cooling obtained for the 45-2-2 (Fig. 15(a)) and 47-2-2-1 (Fig. 15(b)) alloys. For both

materials, the individual reaction curves are labeled according to the following designation for the γ decompostion product: lamellar – γ_L, cellular – γ_C, feathery – γ_F, Widmanstatten – γ_W and massive – γ_M. The data are grouped by the microconsituents observed, irrespective of whether the reaction occurred during continuous-cooling or isothermal treatment. All samples were cooled to the designated temperature, aged if required, then water quenched. The transformation finish curve was also estimated for the fully lamellar transformation in the 45-2-2 alloy. Continuous-cooling-transformation experiments performed by the techniques described here only permit sampling of the α decompostion reaction in the cooling rate range from ~20°C/s and slower, except for water quenching. However, as the experiments show, several of the reactions occurring at high temperature are only suppressed by much more rapid cooling conditions in the 47-2-2-1 alloy. From our cooling rate calculations and experimental observations, both AC (~16.5°C/s) and SPQ (~12.5°C/s) of a 10 mm cube were too slow to suppress these reactions. For this reason, dashed lines are used to describe many reaction regimes. The lines are inferred from experimental observations derived from both continuous cooling and isothermal treatments, which could not be distinguished at short times or for these experimental conditions. Examination of Fig. 15 also reveals that lowering the Al (45-2-2 vs. 47-2-2-1) is effective in delaying the lamellar reaction. The massive γ_M start temperature is not affected much at the cooling rates where it can form, though this transformation mode could be suppressed entirely in the 45-2-2 alloy by water or oil quenching compared with the 47-2-2-1 alloy; this feature is again due to the higher Al concentration in the latter alloy.

Limiting Reactions: Massive and Cellular

The $\alpha \rightarrow \gamma_M$ massive transformation is a composition-invariant, structural change involving short-range diffusion across parent-product interfaces, which is now well documented for binary gamma alloys [18-21,24-29]. The reaction typically nucleates at grain corners, edges and faces and proceeds with high growth velocities into the untransformed α phase, once the massive start temperature is reached. Estimates now place this temperature at a typical undercooling of ~150 -

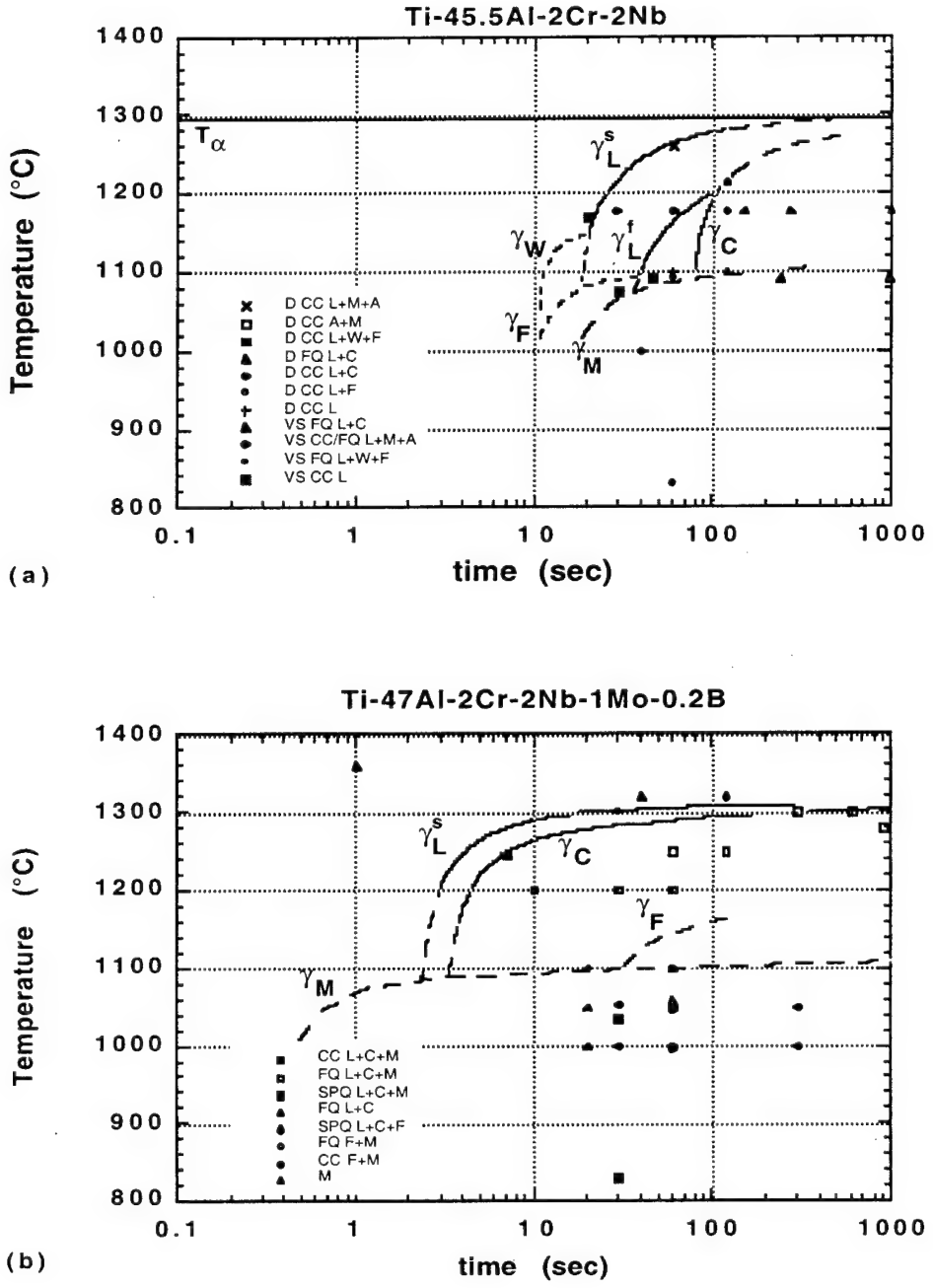

Figure 15. Continuous cooling transformation diagrams for the (a) 45-2-2 and (b) 47-2-2-1 alloys. Data indicated by solid symbols in (a) are taken from the Seetharaman and Semiatin [23] who conducted studies on the same forgings.

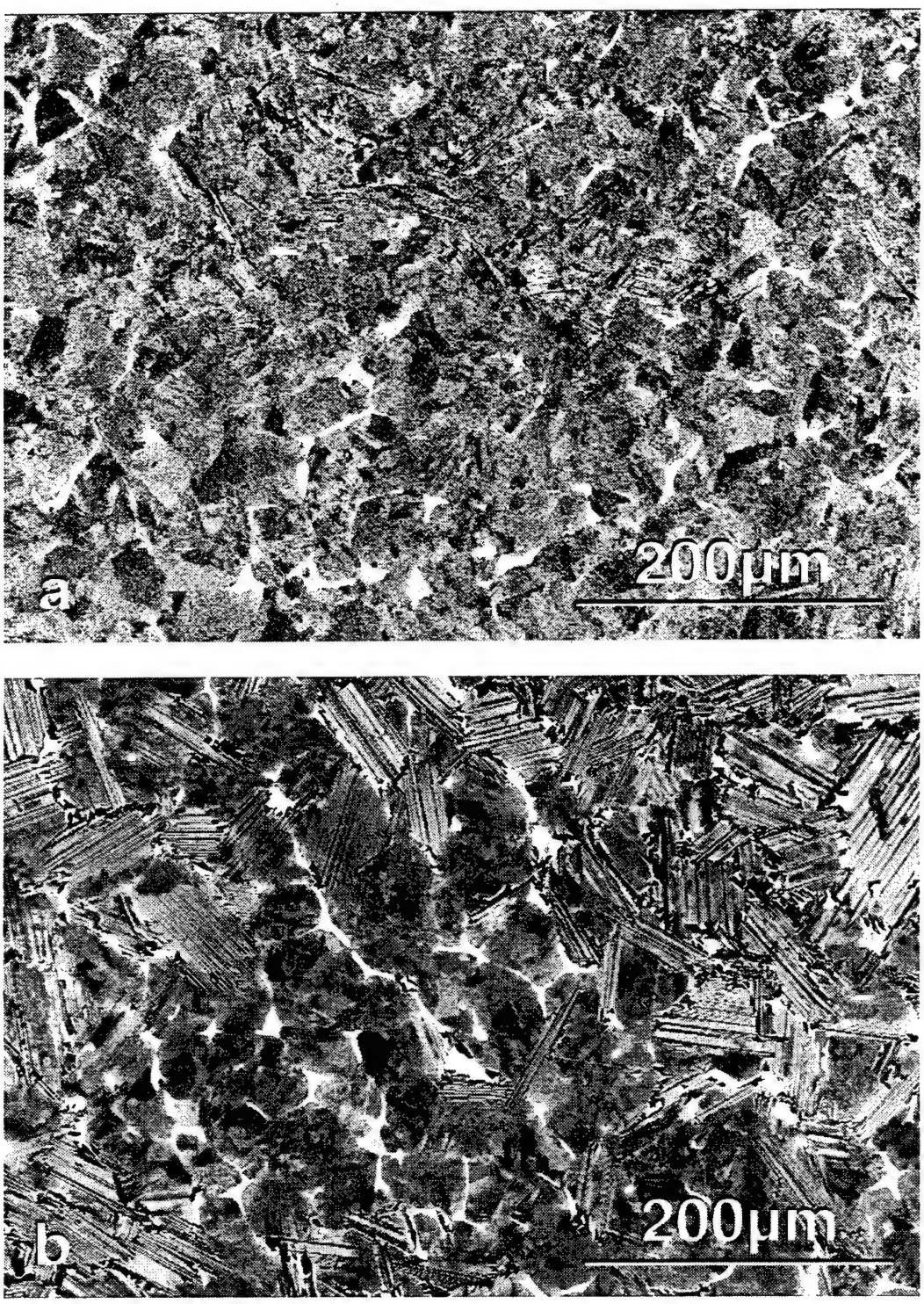

Figure 16. Backscattered electron micrographs of the 47-2-2-1 alloy: (a) γ_M + β, 1370°C/15min.+1300°C/30sec/WQ, and (b) γ_M+γ_L+β 1370°C/15 min + 1200°C /30sec/WQ. Massive-gamma phase (γ_M) is equiaxed gray background, β-phase is imaged light.

200°C below the T_o temperature indicating equal free energies for α and γ phases. For the alloys studied, γ_M start temperature is ~1100°C, but drops slightly with increasing cooling rate. For the 47-2-2-1 alloy, the γ_M microconstituent was observed along with the β phase for samples quenched from temperatures above 1300°C (Fig. 16(a)). The γ_M microconstituent occurred together with γ_L and γ_C constituents for partial transformation at lower temperatures (Fig. 16(b)). The γ_M constituent is also observed under conditions of step quenching + isothermal aging, Figs. 17 and 18. Comparing the two diagrams in Fig. 15, one may observe the important influence of the Al-content of the alloy in providing a chemical driving force for γ_M formation. For the 45-2-2 alloy, the γ_M microconstituent was generally not observed, and the formation curve in Fig. 15(a) is shifted to longer times relative to that in Fig. 15(b). Only water quenching produced trace amounts of γ_M at some grain triple points. Generally such rapid cooling led to retained α phase. Another study showed that for this alloy quenched-α structures consist of the ordered α_2 phase, and they may be aged in the temperature range from 600-800°C to form ultra-fine lamellar microstructure [30].

As cooling rates decrease, α decomposition occurs by alternative reactions which, at the slowest cooling rates, are cellular reactions of several types. As previous studies show [31,32], discontinuous coarsening reactions occur when lamellar microconstituents are slow cooled or exposed to high temperatures for prolonged periods. Examples of these are shown for the 47-2-2-1 and 45-2-2 alloys in Figs. 19(a) and 19(b), respectively. However, in the slow cooling-rate limit, α phase may decompose directly via a cellular reaction involving nucleation and growth of gamma phase at grain boundaries. An example result of such a reaction is shown for the 47-2-2-1 alloy in Fig. 20. Again comparing the two diagrams, the results show that lowing the Al-level shifts the cellular reaction start temperatures to longer times, and expands the range of temperatures between γ_L start and γ_C start. For the 47-2-2-1 alloy, the range between these two temperatures is reduced such that fully lamellar microstructures cannot be produced for this alloy. Such structures are interrupted by rapid cellular growth of gamma from the grain boundary regions (Fig. 19).

(a)

(b)

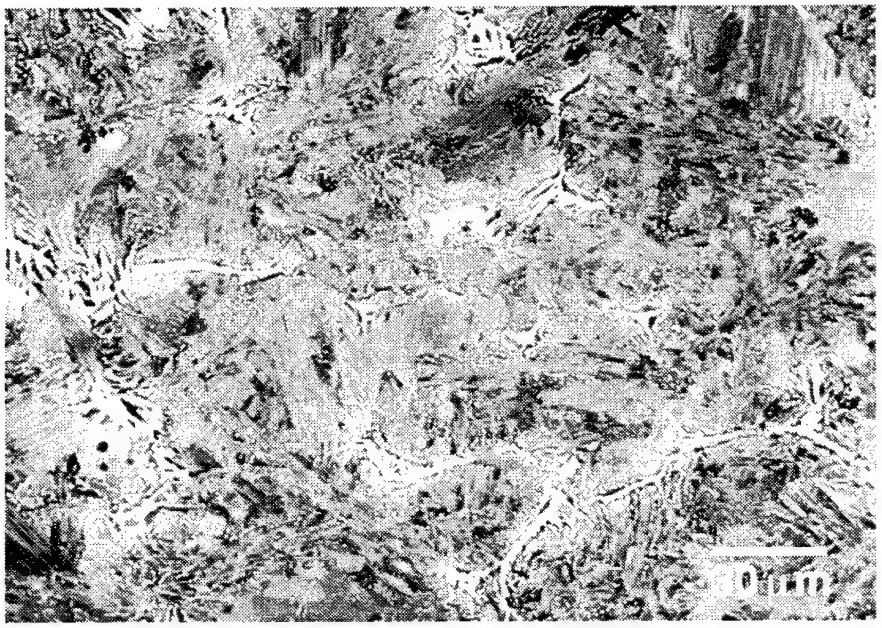

Figure 17. Backscattered electron micrographs of the 47-2-2-1 alloy: (a) $\gamma_M + \gamma_F + \gamma_C + \gamma_L + \beta$, 1370°C/10min. → SPQ 1053°C/5sec/WQ, and (b) $\gamma_M + \gamma_F + \gamma_C + \beta$, 1370°C/10min. → SPQ 1053°C/300sec/WQ. The gray background is a mixture of γ_M, γ_F, γ_L. β-phase is imaged light, $\gamma_C + \beta$ appear as the discontinuously growing product from near the grain boundary β films into the grain interior.

Figure 18. BF TEM micrograph showing the massive γ_M phase/microconstituent in the 47-2-2-1 alloy heat treated according to 1370°C/10min. → SPQ 1053°C/5sec/WQ.

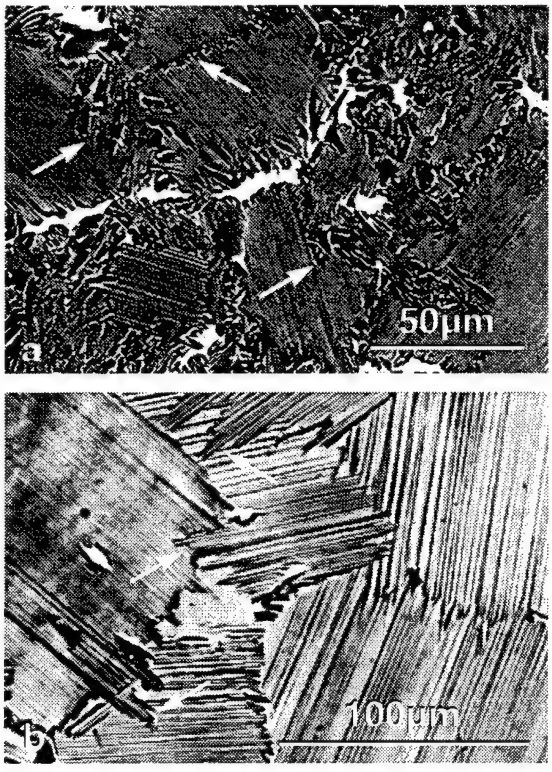

Figure 19. Backscattered electron micrographs of discontinuous coarsening reactions in (a) the 47-2-2-1 alloy after 1370°C/15min. + CC/20°C/sec to 1100°C/20sec/WQ, and (b) 45-2-2 alloy after 1320°C/ 2min. + FC/2min to 1215°C/WQ.

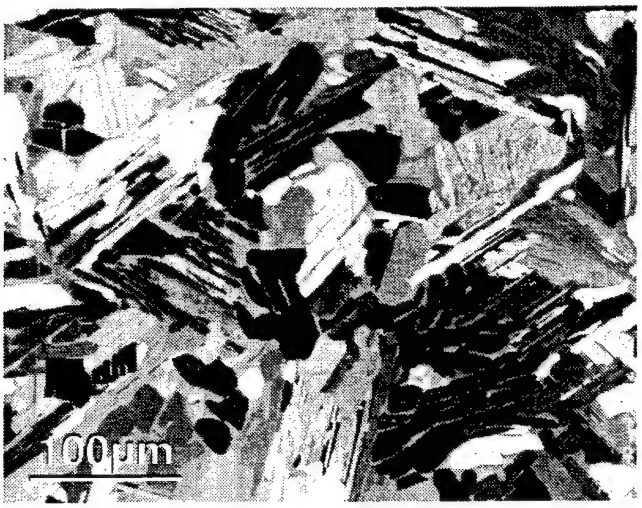

Figure 20. Optical micrograph of 47-2-2-1 alloy heat-treated at 1370°C/15min. + CC/ 0.033°C/sec to 1250°C/AC.

Intermediate Reactions: Lamellar, Widmanstätten and Feathery Lamellar

The transformation of the high-temperature α to lamellar $\alpha_2 + \gamma$ phases has been well known in gamma alloys since the work of Blackburn [33]. Studies from that time indicated that the reaction occurred by spreading of Shockley partial dislocations (stacking fault instability) on the basal planes of the HCP α phase to form the correct stacking sequence for the $L1_0$ structure, followed by diffusional growth and chemical equilibration of the γ phase. This reaction was believed to occur at the eutectoid temperature. Later, others [20,31,34,35] demonstrated that lamellar formation occurred at much higher temperatures in the two phase $\alpha+\gamma$ phase field, and that the reaction exhibits characteristics of a nucleation and growth process, very likely involving diffusion. The results presented in Fig. 15, along with prior kinetic studies shows that lamellar formation occurs quite rapidly below T_α; however, the degree of undercooling required for nucleation of the reaction is strongly dependent upon cooling rate and alloy composition. For the 47-2-2-1 alloy, undercoolings are always greater than 30°C, even at the slowest cooling rates. For this alloy, nucleation may be restricted by the presence of the β-phase regions (films) on the grain boundaries. Lamellar formation is also affected by the grain size of the

parent α phase as discussed previously [36]. As shown by the micrographs in Fig. 21 for the 45-2-2 alloy, larger grain sizes extend the nucleation period for lamellar structures to longer times. Both samples were solution treated above T_α, but for varying times so as to vary the degree of grain growth. Following a treatment, both samples were air cooled for 20 sec to the lamellar start temperature, then water quenched. Figure 21(a) shows that lamellar formation began, but was incomplete, thus allowing the γ_F and γ_M microconstituents to form on further cooling. However, for the larger grained sample shown in Fig. 21(b), lamellar formation did not begin and the resulting structure is retained α with trace amounts of γ_M.

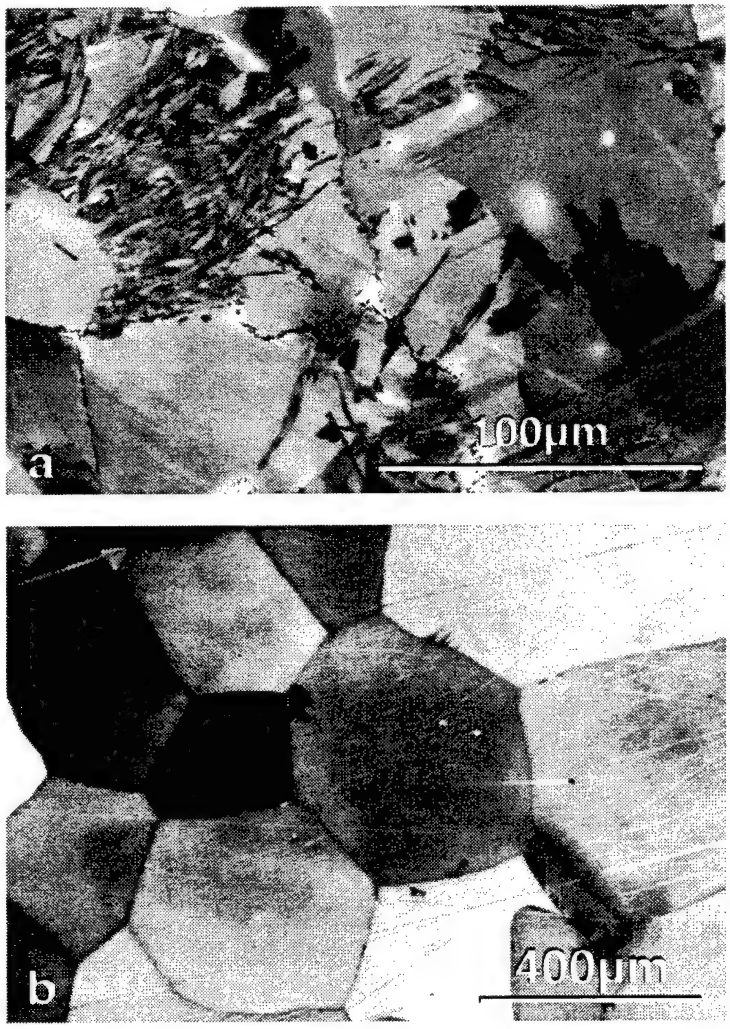

Figure 21. *Backscattered electron micrographs showing effect of grain size on nucleation of alpha-phase decomposition reactions in 45-2-2 alloy; (a) after 1320°C/15min. + AC/20sec to 1170°C/WQ (lamellar start temperature); (b) after 1320°C/60min. +* AC/20sec to 1170°C/WQ.

For selected conditions, α-phase decomposition is also known to occur by disrupted lamellar reactions commonly referred to as Widmanstätten structures (γ_W) [18-21,24-26]. In the present study, γ_W structures were rarely observed, with only trace amounts occurring in a large-grain material cooled at a rate of ~16°C/sec (Fig. 22). However, in the previous investigation by McQuay *et al.* [20], the γ_W structure was quite common for large grained ternary Ti-48Al-2Cr and 3Cr alloys. Note that these ternary alloys, and the alloys described in most literature reports of γ_W structures contain significantly greater levels of Al than the present alloys. These observations and prior literature data indicated that the γ_W start curve exists in close proximity to the γ_L-start curve, and very likely at temperatures higher than the nose of the γ_C-start curve.

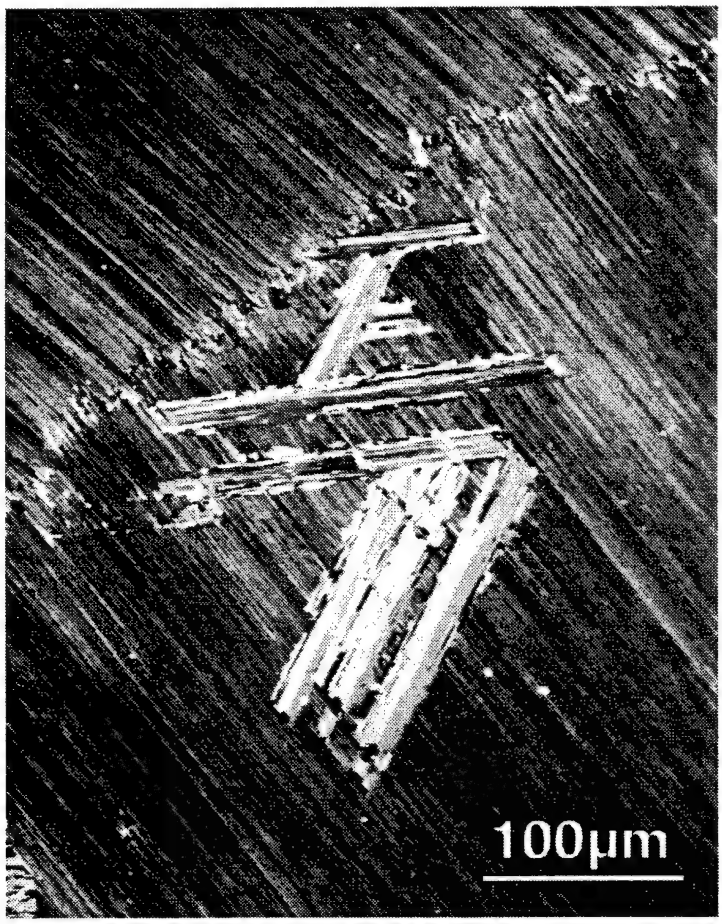

Figure 22. Polarized light optical micrograph of 45-2-2 alloy heat treated at 1320°C/60 min. + 1100°C/60sec/WQ, showing Widmanstätten γ lamellae.

While the exact mechanism for γ_W formation remains unknown, two possibilities have been considered regarding the grain-size and temperature dependencies to γ_W start. First, the fact that γ_W colonies consist of $\alpha_2+\gamma$ lamellar structure, similar in form to the perfect lamellar structure, suggests that they should be crystallographic derivatives of the parent α-phase, but with rotated basal planes. This might occur by deformation of the parent α phase at high temperatures, perhaps by twinning, as is known to occur for selected quenching conditions [37]. Further, one may expect that larger grain sizes would lead to higher local stresses (larger displacements for a given strain) from thermal expansion anisotropy of the α phase during cooling. These may provide a twinning stress; however, the crystallography of γ_W structures is not yet investigated and such stresses are not bounded. Secondly, large grain sizes delay the nucleation of lamellae to greater undercoolings, as shown previously, thus providing increased chemical driving forces and more time for other diffusional processes to occur. Such a nucleation barrier, together with greater opportunity for growth, may permit nucleation and growth of γ_W colonies on habit planes other than the α-phase basal plane. Again, the necessary crystallographic data to distinguish these possibilities has not been obtained.

Another intermediate reaction commonly observed from α-phase transformation is the γ_F Bainite-like microconstituent, sometimes referred to as fine Widmanstätten or acicular structure [18-21,29,38]. The cooling curves in Fig. 15 indicate that the structure is obtainable for the compositions studied. Figure 21(a) shows an example of this structure for the 45-2-2 alloy; the same microconstituent forms in the matrix of the 47-2-2-1 alloy as shown in Figs. 23(a,b) and 24. For the 47-2-2-1 alloy, the volume fractions of γ_F microconstituent were greater than ~30% for samples SPQ and aged at temperatures of 1050°C or less, and aging times greater than 60 sec. For these cooling treatments, it is believed that the γ_F structure formed upon cooling, at temperatures greater than the γ_M start curve. For the 45-2-2 alloy, the γ_F microconstituent was commonly formed for cooling rates which prevented crossing the γ_C start and γ_L finish curves shown in Fig. 15. Thus, for this alloy, it is likely that the γ_F microconstituent forms before the γ_M start.

(a)

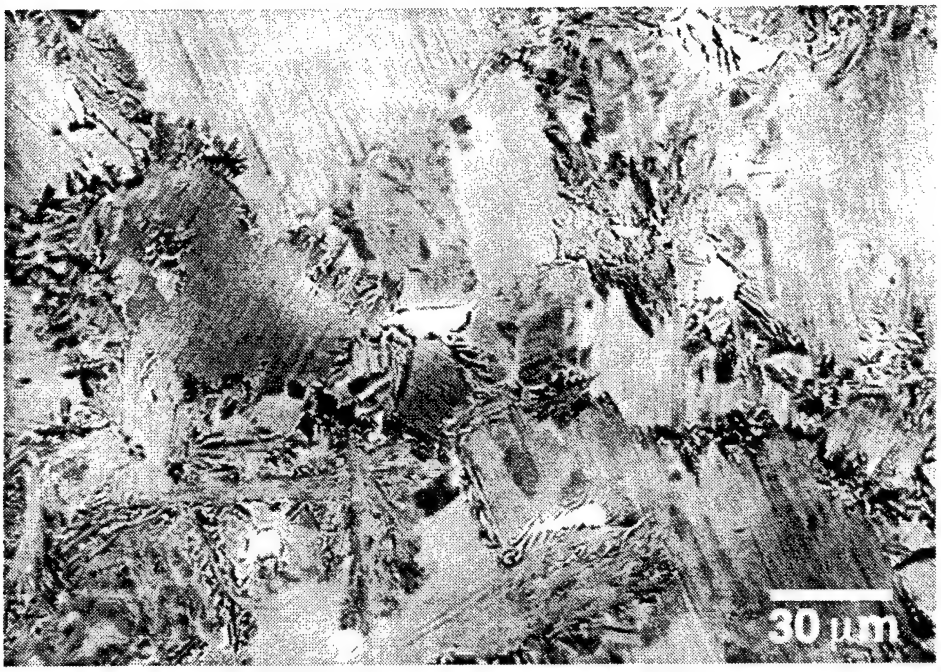

(b)

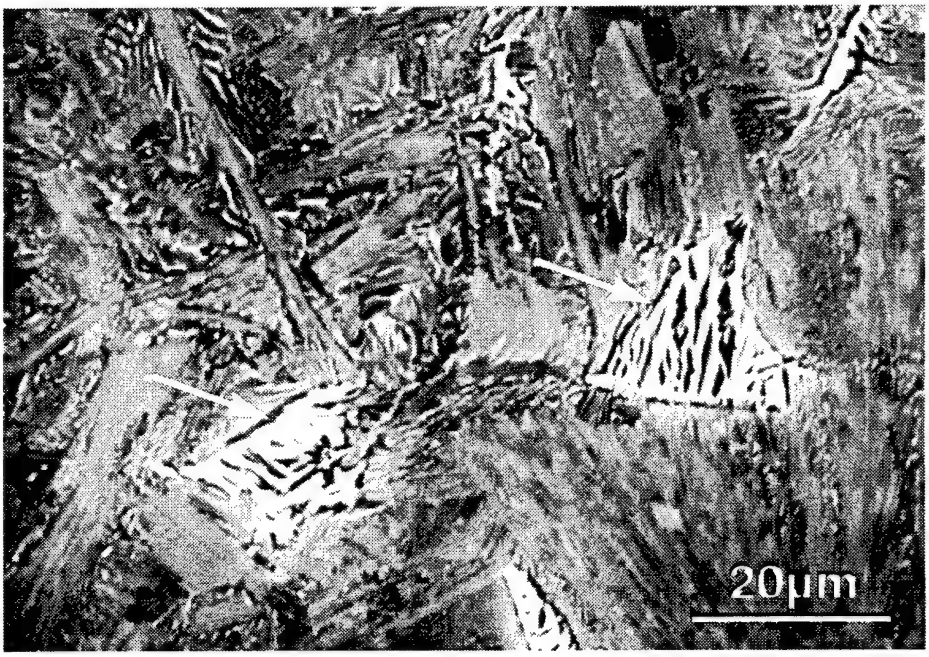

Figure 23. Backscattered electron micrograph showing beta and alpha phase cellular decomposition reactions in 47-2-2-1 alloy. : (a) γ_M + γ_F +γ_C +γ_L + β, 1345°C/10min. → SPQ 1000°C/5sec/WQ, and (b) γ_M + γ_F +γ_C +γ_L + β,1370°C/10min. → SPQ 1000°C/60sec/WQ. The gray background is a mixture of γ_M, γ_F, γ_L. β-phase is imaged light, γ_C + β appear as the discontinuously growing product from near the grain boundary β films into the grain interior.

TEM investigation of this feathery structure indicates that it consists of a fine lamellar-plate colony structure of $\alpha_2+\gamma$ phases, and does not have an acicular morphology (Fig. 24). The lamellar colonies have a similar size scale (~0.5-5.0μm) as the variants of γ phase observed after γ_M formation. Further, these lamellar colonies tend to form having a range of colony-to-colony misorientations commonly of less than ~15°. However, within the colonies, lamellar structures have a common crystallographic orientation to the α_2 phase. The α_2 phase tends to exhibit an irregular thickness or interface habit plane.

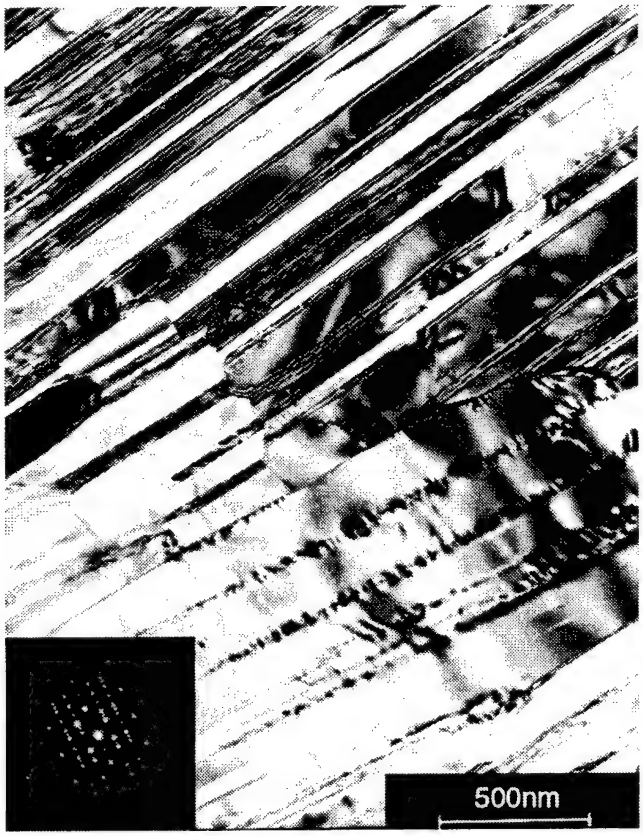

Figure 24. TEM Bright-field micrograph of feathery gamma (γ_F) microconstituent in 47-2-2-1 alloy. Lamellae viewed edge-on for colony in lower left (<101] diffraction pattern), other colonies show small misorientations.

For this reaction, again two possible mechanisms are being investigated. One possibility is that the γ_F product results from deformation of the α phase just prior to or during the

transformation, causing small misorientations and low-angle boundaries, in the α-phase ahead of a transformation front. Such deformed α regions would subsequently transform to γ_F lamellar colonies after the reaction front passes. One may expect that nucleation of coherent γ-phase lamellae in a grain results in large coherency stresses, in addition to thermal expansion anisotropy stresses, which may locally lead to buckling or distortion of the α phase. Alternatively, the possibility of a γ_M transformation front passing through the α phase, together with diffusional precipitation of α in γ phase, cannot be ruled out.

Additional TEM observations (Fig. 25) reveal that the γ_F is closely related to a discontinuous nucleation and growth process. The observations indicate that α_2+γ lamellae packets formed in one grain nucleate new packets that fan out and grow into neighboring parent α grains past the grain boundaries, with no apparent low-index orientations or crystallographic impediments relative to the grain into which nucleation and growth occurs. Once again, extensive documentation of the crystallographic and chemical nature of the transformation products are required to further clarify the formation mechanisms. Taken together, the γ_W, γ_F, and γ_L transformation paths have many characteristics of Upper and Lower Bainite, and Pearlite formation in steels, respectively. Unfortunately, the reaction temperatures are sufficiently high, with reaction times so short, that experimental elucidation of their formation mechanisms remains difficult.

Beta-Phase Decomposition

For the 47-2-2-1 alloy, and similar alloys exhibiting three-phase α+γ+β phase equilibria, one other high-temperature reaction must be considered. For such alloys a single-phase α field may not exist, and decomposition of the high-temperature β phase occurs as well as α decomposition (Figs. 16, 23). The reaction appears to be the cellular transformation β—>γ+β, or β—>γ+β+α, and appears in two morhological forms: the first as coarse γ precipitates within coarse grain boundary β films (Fig. 26(a)), and the second as a cellular product comprised of alternating γ and β lamellae (Fig. 26(b)). In both cases the β phase had ordered to a B2 structure and held a Burgers orientation relation, with the precipitated γ, viz. (011) B2 // (1$\bar{1}$1) γ, [111] B2 // [011] γ.

(a)

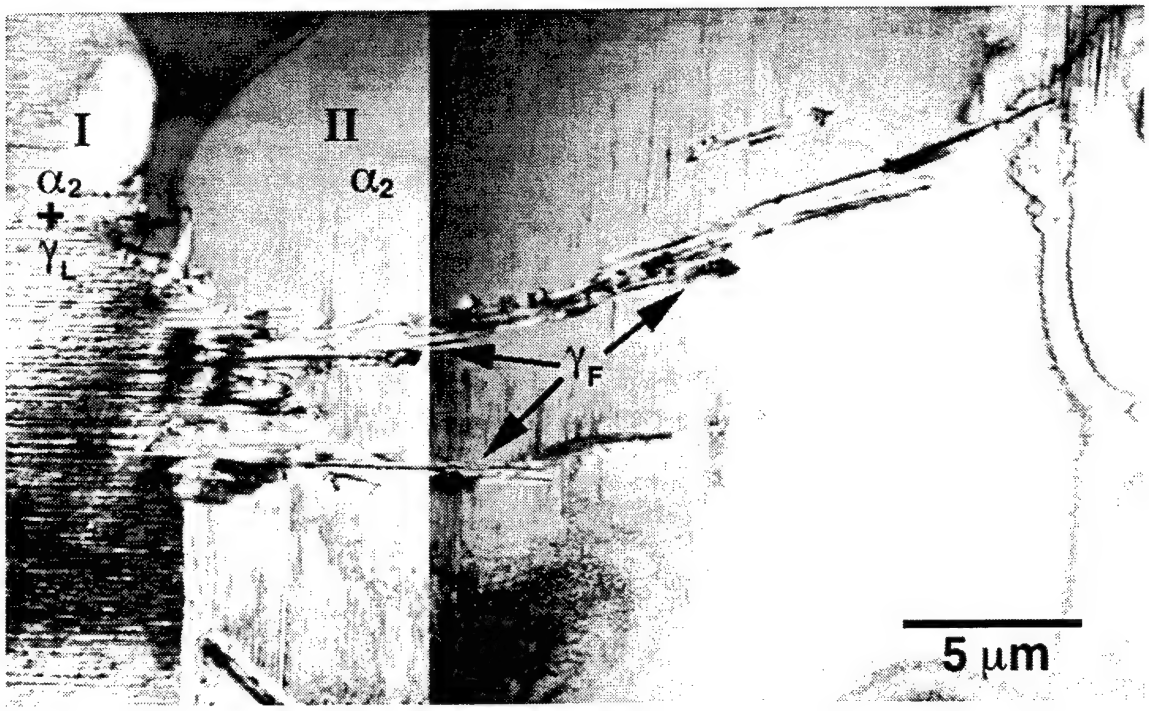

(b)

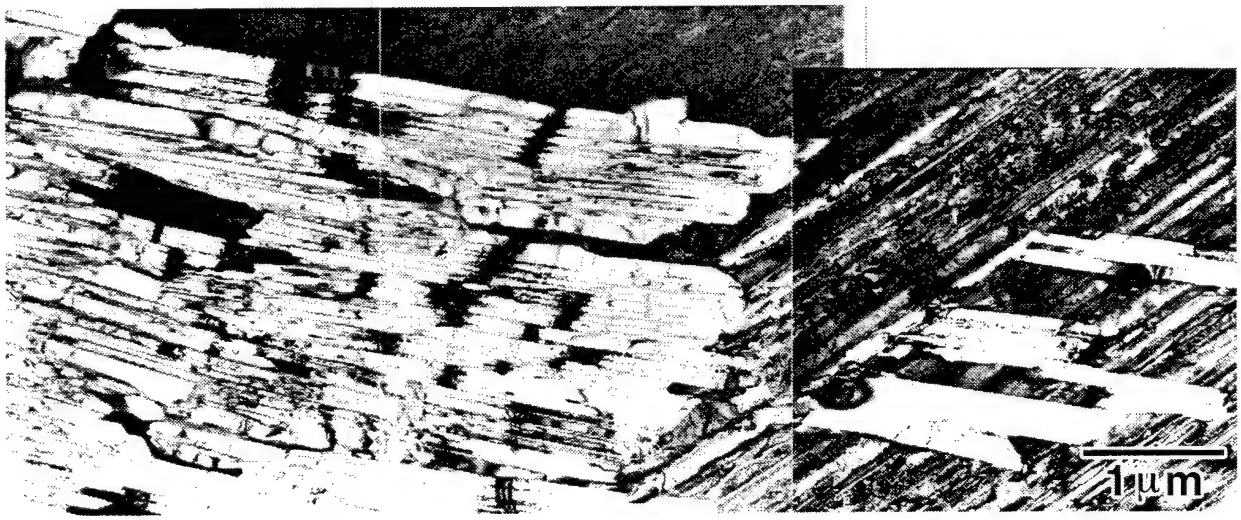

Figure 25. TEM bright-field micrographs of feathery gamma (γ_F) microconstituent in 45-2-2 alloy (heat treated according to 1320°C/15min. + AC/20sec to 1170°C/WQ. The lamellar γ_L front from one grain grows into a neighboring parent alpha grain discontinuously and fans out in the form of the feathery γ_F microconstituent.

(a)

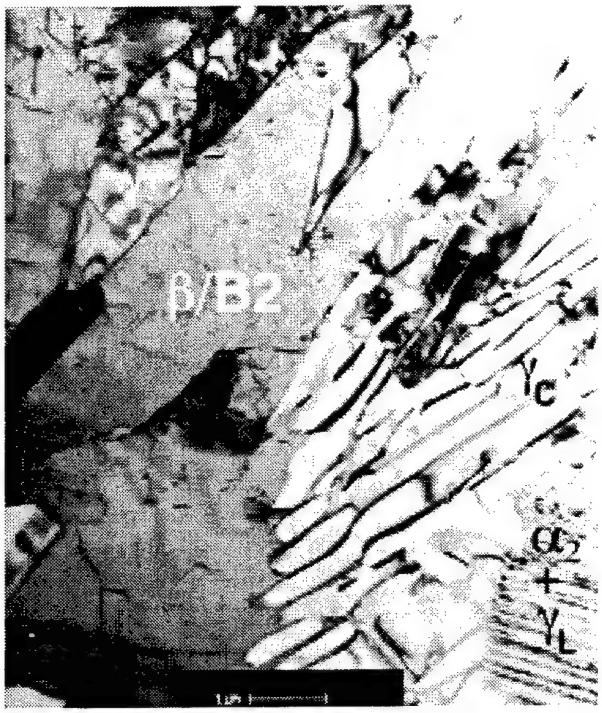

(b)

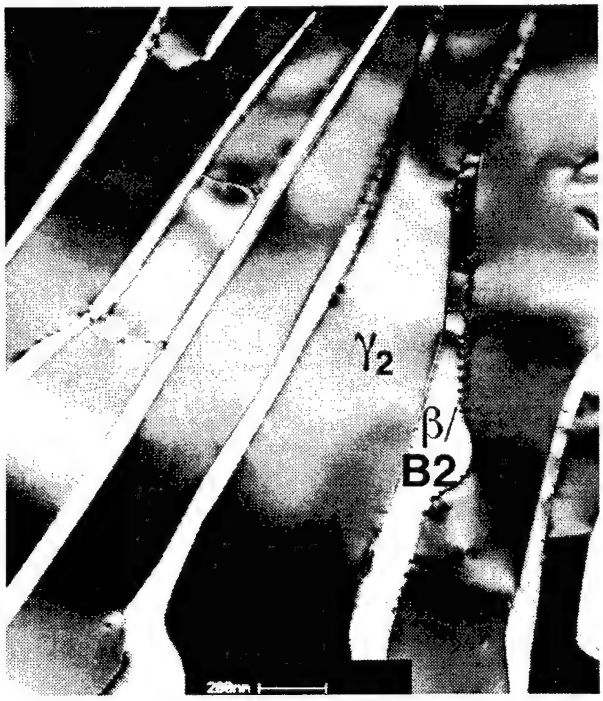

Figure 26. TEM micrographs showing beta decomposition products in the 47-2-2-1 alloy heat treated according to 1370°C/10min. → SPQ 1053°C/5sec/WQ. (a) Coarse γ precipitates in grain boundary β/B2 and (b) cellular γ_C + β/B2 product.

This transformation is driven by the decreasing solubility for Al in β with decreasing temperature (Table 6), and increasing the isothermal aging time considerably enhances the extent of the cellular product. For such alloys, this reaction may be quite important in facilitating nucleation of the γ_C microconstituent. In the 47-2-2-1 alloy the reaction was so prevalent that fully lamellar microstructures could not be formed. The reaction start temperature was observed to be lower than the γ_L start temperature, and is estimated to be below 1200°C (compare β phase in Figs. 16(b) and 23). In some cases, the β/B2 phase was also present in the form of small platelets within regions of massive γ_M (Fig. 27(a)) and with the same Burgers orientation relation (Fig. 27(b)).

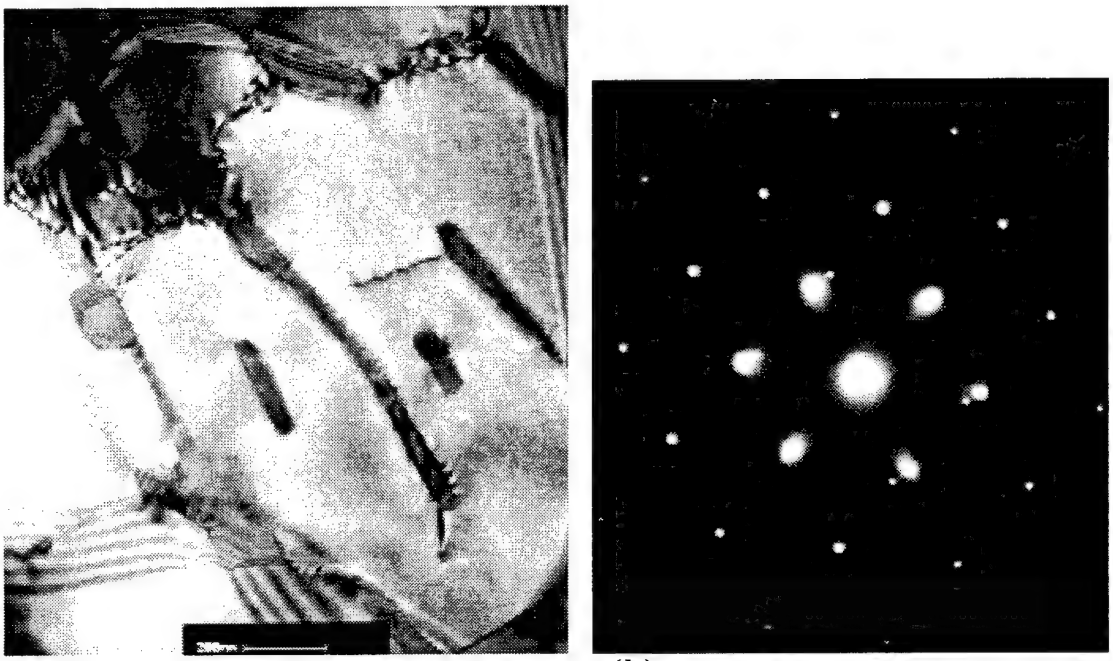

Figure 27. TEM micrographs showing β/B2 precipitates in massive γ_M in the 47-2-2-1 alloy heat treated according to 1345°C/10min. → SPQ 1000°C/30sec/WQ. (a) BF micrograph and (b) [101] γ// [111] β/B2 SAD pattern

Phase/Constituent Chemistry

The chemical compositions of the various phases in the different morphological products observed in the heat treated 47-2-2-1 alloy, determined through EDS in the TEM using an established standard, are shown in Table 6. As can be seen, the β/B2 phase (in various forms) has reduced solubility of Al, but considerably enhanced levels of Cr and Mo compared with the bulk

alloy compostion. In contrast, the γ_L and γ_F products have high Al, but low Cr and Mo relative to the bulk. The α_2 has an Al content slightly higher than that in the β/B2, but Cr and Mo levels slightly higher than those seen in the γ_L and γ_F. The massive γ_M chemistry is close to that of the bulk alloy composition, as expected. The Nb content in all the phases is more or less the same and near that of in the bulk alloy, which indicates this element partitions equally in the α, β and γ phases. On occasion, a few particles with very high levels of Nb, and reduced Al, Cr and Mo levels were observed. The structure of these particles has not been determined. It is clear that the reduced solubility limits for Al and increased solubilities of Cr and Mo in the β-phase drives its transformation to the non-lamellar γ products.

TABLE 6: Composition (in at.%) of the Phases in Various Forms in the Ti-47-2-2-1 Alloy

Heat-treatment	Phase/Constituent*	Ti	Al	Nb	Cr	Mo
1370°C/10min → SPQ 1053°C/5sec/WQ	Coarse GB B2	52.90	38.33	2.62	4.30	1.80
	Coarse GB γ	47.65	47.75	2.27	1.50	0.83
	Cellular B2	52.19	35.53	2.72	6.72	2.85
	Cellular γ	46.50	48.82	2.19	1.51	0.99
	Lamellar γ	46.66	48.86	2.27	1.39	0.92
	Lamellar α_2	51.39	39.84	2.23	2.80	1.29
	Feathery γ	46.90	48.48	2.04	1.88	0.71
	Massive γ	47.88	46.90	2.38	1.92	0.92
	B2 Ppt in Massive γ	54.00	33.23	2.53	6.98	3.37
1370°C/10min → SPQ 1053°C/300sec/WQ	Coarse GB B2	51.58	36.81	2.97	6.42	2.42
	Coarse GB γ	47.39	47.68	2.45	1.67	0.82
	Cellular B2	50.91	35.69	2.61	7.10	3.72
	Cellular γ	47.00	48.00	2.41	1.77	0.78
	Lamellar γ	48.65	46.05	2.53	1.99	0.79
	Lamellar α_2	53.96	40.15	2.95	1.95	1.00
	Massive γ	47.86	47.06	2.33	2.99	0.77
	Ppt in Massive γ	43.52	33.42	21.35	1.22	0.48
1345°C/10min → SPQ 1000°C/5sec/WQ	Massive γ	48.44	46.59	2.22	1.93	0.84
	B2 Ppt in Massive γ	54.66	34.07	2.39	6.72	2.17
	Ppt in Massive γ	42.25	32.92	23.23	1.21	0.39

Comparison With Binary and Ternary Alloys

Figure 28 shows only the γ_L start curves for binary Ti-47.9Al, Ti-47.5Al, Ti-46.5Al, ternary Ti-48Al-2Cr, and the two alloys from this study. The data for binary alloys are from Vasudevan et al. [18,21,39], while that for Cr-containing material is from the data of McQuay [20]. The comparison shows that changes in the Al-level and transition metal alloying additions are equivalently effective in delaying the onset of lamellar transformation, allowing the reaction to be controlled at slower cooling rates. This is important for developing lamellar structures in engineered components. However, effective design of fully lamellar materials with good creep resistance also requires suppression of the cellular reactions occurring at longer times for most alloys. For this, several factors are anticipated to be important. First, the chemical driving forces for formation of the γ_C microconstituent must be reduced by both lowering the Al-levels from the Ti-48Al base, and by reducing the β-forming elements of Cr, Mo, and W. The elements Nb, Ta, and V may also be important for this reason. Further, the surface-energy barriers for non-lamellar constituents must be increased by reducing the misfit parameters (strain/interfacial energies). For this, the experimental data base is essentially nonexistent. Future progress in developing stable fully lamellar gamma alloys will depend on control of these variables and may benefit from advances in computational prediction of misfit parameters and phase stability.

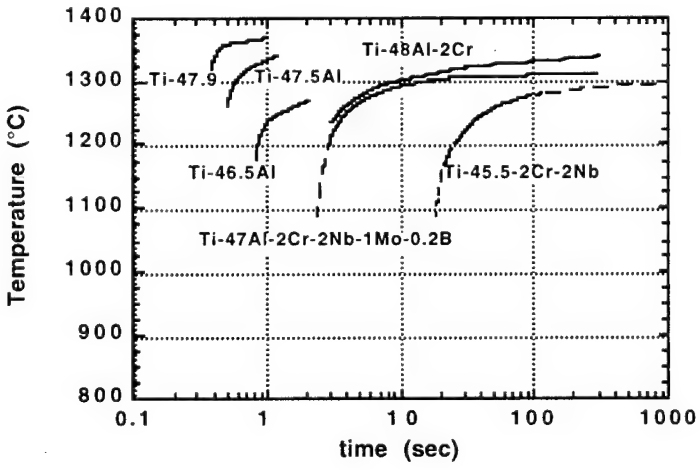

Figure 28. The γ_L start curves for binary Ti-47.9Al, Ti-47.5Al, Ti-46.5Al, ternary Ti-48Al-2Cr, and the Ti-47-2Cr-2Mo-2Nb-0.9Mo-0.2B and Ti-45.5Al-2Cr-2Nb alloys.

4. CONCLUSIONS

The following are the major new findings resulting from the work on this project.

Nb-Ti-Al Alloys

1. The sequence of phase transformations in the 37Nb-37Ti-26Al alloy have been established, together with tie lines at a number of temperatures between 1000 to 1300°C.
2. The O phase is found to be the stable phase at temperatures <1000°C, with $\beta+\sigma$ being the stable phases between 1000 to 1325°C and only β above 1325°C.
3. A composition invariant, displacive/martensite-like B2→O transformation has been observed.
4. ALCHEMI results reveal that in the B2 phase (i) Al and Ti occupy two different, (ii) Nb partitions to both Al and Ti sites but prefers the Ti sites, and (iii) formation of Ti antisite occurs. On the other hand, in the O phase the Nb atoms tend to separate from Al and show a preference to occupy the Ti sites.

Multicomponent Gamma Titanium Aluminides

1. The microstructures of the cast alloys show evidence of: $L \rightarrow L + \beta \rightarrow \alpha + \beta$ cores $\rightarrow$ lamellar $(\alpha + \gamma) + \beta$ cores $\rightarrow$ lamellar $(\alpha_2 + \gamma) +$ B2 cores, solidification and transformation pathway; and in the alloys with boron, ribbon-like borides that have formed directly in the liquid are also present.
2. The borides were determined to be TiB_2 and found to contain thin, interleaving layers of the B2 phase with the orientation relationship: (100) B2 // $(10\bar{1}0)$ TiB_2, [001]B2 // [0001] TiB_2.
3. In the boron-free alloys heat treated above 1360°C, the β phase is present as a thick continuous film along the prior α grain boundaries along with several variants of the γ phase, which provides evidence for direct formation of γ from β. With boron additions, the volume fraction of the β/B2 phase reduces such that it is mainly found as small particles at the prior α grain boundaries.

4. In the B-free alloys, the feathery/massive γ morphologies are favored over the lamellar morphology as the transformation product of the α phase. In contrast, B addition to the alloys has the dramatic effect of restricting α grain growth, of promoting the lamellar γ morphology and lamellar growth and of suppressing the non-lamellar/feathery/massive γ mode of transformation. It is perceived that due to the finer grain size of the prior α grains the lamellar transfor-mation can begin at smaller undercoolings and go to completion before the samples have cooled sufficiently below the α/γ T_o temperature to allow non-lamellar morphologies to appear.

5. ALCHEMI results show that Al and Ti occupy different lattice sites in the B2 phase and that both Cr and Mo atoms have a strong preference for the Al sites. These results also seem to be borne out in the compostion determined for the B2 phase, which shows that the Ti concentration is ~50 at.% and the sum of Al, Cr and Mo roughly make-up the remaining 50%, with Nb probably distributed more on the Ti than Al sites.

6. The reaction sequences for alpha-phase decomposition in gamma alloys was quantified. Special emphasis was placed on quantifying the heat transfer conditions used in the experimental study. The results lead to partial CCT diagrams for two multicomponent alloys that describe the temperature, time dependence of the various reaction modes.

7. Limiting reaction sequences in gamma alloys are massive gamma formation and cellular gamma formation at the highest and lowest cooling rates, respectively.

8. Intermediate reaction products consist of $\gamma_L+\alpha$, $\gamma_W+\alpha$, and $\gamma_F+\alpha$, depending upon the alloy composition, cooling rate and grain size. The formation mechanisms and nature of the γ_W and γ_F microconstituents have been proposed.

9. Decompostion of the high temperature β phase is found to take two forms: precipitation of coarse γ within grain boundary films and as a cellular reaction leading to alternate γ and β lamellae. This reaction is driven by the reduced solubility of Al and increased Cr and Mo

solubilities in the β phase with decreasing temperature. The β phase is found to have undergone ordering to a B2 structure, in which Ti atoms occupy one site, the Al, Cr and Mo atoms the other site and Nb partitioning about equally to both sites.

10. Both the Al-level and the degree of transition-metal alloying can lead to marked (both favorable and unfavorable) shifts in the kinetic windows of formation of the various microconstituents. Reducing the Al-level and β-phase forming elements tends to mitigate unfavorable decomposition via cellular reactions.

5. REFERENCES

1. V. K. Vasudevan, K. J. Leonard and J. C. Mishurda, "A Study of the Kinetics of Phase Transformations in the Nb-Ti-Al System," *AFOSR Grant No. F49620-95-1-0487*, **Final Report**, June 19 (2000).
2. J. H. Perepezko, Y.A. Chang, L.E. Seitzman, J.C. Lin, N.R. Bonda, T.J. Jewett and J.C. Mishurda, *in: High Temperature Aluminides and Intermetallics*, ASM, Materials Park, OH, 19 (1990).
3. U.R. Kattner and W.J. Boettinger, *Mat. Sci. Engng.*, **A152**, 9 (1992)
4. L. A. Bendersky and W. J. Boettinger, *J. Res. NIST*, **98**, 585-606 (1993).
5. D. Banerjee, A. K. Gogia, T. K. Nandi and V. A. Joshi, *Acta Metall.*, **36**, 871-882 (1988).
6. L. A. Bendersky, *Scripta Metall. Mater.*, **29**, 1645-1650 (1993).
7. J. Shyue, D-H. Hou, S. C. Johnson and H. L. Fraser, *In: Structural Intermetallics*, R. Darolia et al. (eds.), TMS, Warrendale, PA, 631-635 (1993).
8. D. H. Hou, I. P. Jones and H. L. Fraser, *Phil. Mag A*, vol. 74, pp. 741-760 (1996).
9. D. G. Konitzer, I. P. Jones, and H. L. Fraser, *Scripta metall.*, **20**, 265 (1986).
10. D. Veeraraghavan and V. K. Vasudevan, *Mater. Sci. Engg.*, **A192/193**, 950 (1995).
11. B. J. Inkson, C. B. Boothroyd and C. J. Humphreys, *Acta Mater.*, **43**, 1429 (1995).
12. B. Godfrey and M. H. Loretto, *Intermetallics*, **4**, 47 (1995).
13. C. McCullough, J. J. Valencia, C. G. Levi and R. Mehrabian, *Acta Metall.*, **37**, 1321 (1989).
14. P. Wang, G. B. Viswanathan and V. K. Vasudevan, *Metall. Trans.*, **23A**, 792 (1992).
15. P. Wang and V. K. Vasudevan, *Mat. Res. Soc. Symp. Proc.*, **288**, 229 (1993).

16. B. J. Inkson, C. B. Boothroyd and C .J. Humphreys, *J. de Physique IV*, **3**, 397 (1993).

17. Y-W. Kim, "Trends in the Development of Gamma TiAl Alloys," in: *Gamma Titanium Aluminides*, Y-W. Kim, R. Wagner, and M. Yamaguchi, eds., TMS, Warrendale, PA, 637-54 (1995).

18. G. Ramanath and V.K. Vasudevan, "The α—>γ Transformation During Continuous Cooling in Ti-48 At% Al Alloys," *Mat. Res. Soc. Symp. Proc.*, **288**, 223-28 (1993).

19. P. Wang and V.K. Vasudevan, "Effect of Cooling Rate on Decomposition of the α Phase in Ti-(43-50) At% Al Alloys," *Mat. Res. Soc. Symp. Proc.*, **288**, 229-36 (1993).

20. P.A. McQuay, D.M. Dimiduk, H.A. Lipsitt, and S.L. Semiatin, "Effect of Chromium on the Kinetics of Alpha Decomposition in Gamma TiAl Alloys," in: *Titanium '92 Science and Technology*, F.H. Froes and I. Caplan, eds, TMS, Warrendale, PA, 1041-48 (1993).

21. D. Veeraraghavan, P. Wang and V. K. Vasudevan, "Kinetics and Thermodynamics of the $\alpha \rightarrow \gamma_M$ Massive Transformation in a Ti-47.5 At.% Al Alloy," *Acta Mater.*, **47**, 3313-3330 (1999).

22. S.L. Semiatin, B. Goetz, and D.M. Dimiduk, AFRL, WPAFB, Dayton, OH, *unpublished research* (1998).

23. V. Seetharaman and S.L. Semiatin, *Metall. Mater. Trans.*, **27A**, 1987-2004 (1996).

24. P. Wang, G.B. Viswanathan, and V.K. Vasudevan, "Observation of a Massive Transformation From α to γ in Quenched Ti-48 At. Pct Al Alloys," *Metall. Mater. Trans.*, **23A**, 690-97 (1992).

25. P. Wang and V.K. Vasudevan, "Composition Dependence of the Massive Transformation From α to γ in Quenched TiAl Alloys," *Scripta Metall. Mater.*, **27**, 89-94 (1992).

26. M. Takayama, T. Kumagai, M. Nakamura, & M. Kikuchi, "Cooling Rate Dependence of the α/γ Phase Transformation in Titanium Aluminides and Its Application to Alloy Development," in: *Structural Intermetallics,* R. Darolia, J.J. Lewandowski, C.T. Liu, P.L. Martin, and M.V. Nathal, eds., TMS, Warrendale, USA167-76 (1993).

27. A. Denquin and S. Naka, "Phase Transformation Mechanisms Involved in Two-Phase TiAl-Based Alloys—II. Discontinuous Coarsening and Massive-Type Transformation," *Acta Metall. Mater.*, 44 (1996), 353-65.

28. X. D. Zhang, Y. G. Li, M. J. Kaufman and M. H. Loretto, *Acta Mater.*, **44**, 3735-3750 (1996).

29. T. Kumagai, E. Abe, and M. Nakamura, "Microstructure Evolution Through the α—>γ Phase Transformation in a Ti-48 At. Pct Al Alloy," *Metall. Mater. Trans.*, **29A**, 19-26 (1998).

30. Y. Q. Sun, "Nanometer-Scale, Fully Lamellar Microstructure in Aged TiAl-Based Alloy," *Metall. Mater. Trans.*, **29A**, 2679-85 (1998).

31. A. Denquin and S. Naka, "Phase Transformation Mechanisms Involved in Two-Phase TiAl-Based Alloys—I. Lamellar Structure Formation," *Acta Metall. Mater.*, **44**, 343-52 (1996).

32. S. Mato and L.A. Bendersky, "Morhology of Discontinuous Coarsening in Fully Lamellar Ti-44Al (at%) Alloy," in: *Structural Intermetallics*, M.V. Nathal, R. Darolia, C.T. Liu, P.L. Martin, D.B. Miracle, R. Wagner, and M. Yamaguchi, eds., TMS, Warrendale, PA, 177-83 (1997).

33. M.J. Blackburn, in: *The Science, Technology and Application of Titanium Alloys*, R.I. Jaffee and N.E. Promisel, eds., Plenum Press, New York, NY 633-43 (1970).

34. S.A. Jones and M.J. Kaufman, "Phase Equilibria and Transformations in Intermediate Titanium-Aluminum Alloys," *Acta Metall. Mater.*, **41**, 387-98 (1993).

35. P.A. McQuay, D.M. Dimiduk, and S.L. Semiatin, "The Decomposition of Alpha Phase During Continuous Cooling and Isothermal Transformation in Gamma Titanium Aluminide," *Scripta Metall. Mater.*, **25**, 1689-94 (1991).

36. L.L. Rothenflue and H.A. Lipsitt, "Time-Temperature-Transformation Behavior of Complex Gamma Alloys," in: *Titanium '95 Science and Technology*, P.A. Blenkinsop, W.J. Evans, and H.M. Flower, eds., The Institute of Materials, London, UK, 176-83 (1996).

37. P. Wang, D. Veeraraghavan, and V.K. Vasudevan, "A First Report on the Observation of Twins in the α_2 Phase in a Quenched Ti-46.54 At. % Al Alloy," *Scripta Mater.*, **34**, 1601-07 (1996).

38. R.V. Ramanujan, "Diffusional and Composition Invariant Phase Transformations in γ-Based Titanium Aluminides," in: *Solid-Solid Phase Transformations*, W.C. Johnson, J.M. Howe, D.E. Laughlin, and W.A. Soffa, eds., TMS, Warrendale, PA, 881-86 (1994).

39. D. Veeraraghavan, P. Wang, U. Pilchowski and V. K. Vasudevan, "Kinetics of the $\alpha \rightarrow \gamma$ Transformation in Ti-(46-48)Al Alloys," in: *The Japan Institute of Metals Proceedings on Solid-Solid Phase Transformations I*, M. Koiwa, K. Otsuka and T. Miyazaki (eds,) Japan Inst. Metals, Kyoto, Japan, vol. 12, pp.149-152 (1999).

6. PERSONNEL SUPPORTED

The personnel supported in this project include Vijay K. Vasudevan (PI), K. Madangopal (post-doctoral research associate August 1, 1996 to August 1, 1997), N. Giridhar and Bharath Natarajan (graduate students).

7. PRESENTATIONS

1. V. K. Vasudevan, "A Study of Phase Equilibria and Transformations in the Nb-Ti-Al and TiAl Systems," *AFOSR Metallic Materials Contractors' Meeting, Materials Workshop*, Bar Harbor, ME, Aug 19-21 (1996).

2. N. Giridhar, K. Madangopal and V. K. Vasudevan, "Microstructure Evolution in a 37Nb-37Ti-26Al Intermetallic Alloy," *Materials Week/TMS Fall Meeting*, Cincinnati, OH, Oct. 7-10 (1996).

3. B. Natarajan, K. Madangopal, V. K. Vasudevan and D. M. Dimiduk, "Microstructural Evolution in Ti-47Al-2Cr-2Nb-1Mo-(0-0.2)B Gamma Titanium Aluminum," *Materials Week/TMS Fall Meeting*, Cincinnati, OH, Oct. 7-10 (1996).

4. B. Natarajan, K. Madangopal, V. K. Vasudevan and D. M. Dimiduk, "Effects of β-Phase Stabilizers and Boron Additions on Microstructural Evolution in Ti-47Al-2Cr-2Nb-1Mo-(0-0.2)B Gamma Titanium Aluminum," *Symposium on High Temperature Ordered Intermetallics VII, MRS Fall Meeting*, Boston, Dec. 2-5 (1996).

5. N. Giridhar, K. Madangopal and V. K. Vasudevan, "Phase Transformations and Microstructure Evolution in a 37Nb-37Ti-26Al Intermetallic Alloy," *Symposium on High Temperature Ordered Intermetallics VII, MRS Fall Meeting*, Boston, Dec. 2-5 (1996).

6. K. Madangopal, B. Natarajan, V. K. Vasudevan and D. M. Dimuduk, "Microstructure Evolution in Gamma Titanium Aluminides Containing Beta-Phase Stabilizers and Boron Additions," *International Symposium on Structural Intermetallics II*, TMS, Seven Springs, PA September (1997).

7. V. K. Vasudevan, "Phase Equilibria and Transformations in the Nb-Ti-Al System," *High Temperature Materials Workshop, Wright Laboratories, Materials Directorate, WPAFB*, Dayton, OH, Oct. 15-16 (1997).

8. K. J. Leonard and V. K. Vasudevan, "Solidification Pathways and Solid State Transformations in Nb-Ti-Al Alloys," *Symposium on New and Emerging Applications for Refractory Metals and Materials*, TMS, Rosemont, IL, Oct. (1998).

9. K. J. Leonard and V. K. Vasudevan, "Decomposition of the β Phase in a Nb-25Ti-25Al Alloy," *Symposium on New and Emerging Applications for Refractory Metals and Materials*, TMS, Rosemont, IL, Oct. (1998).

10. J. C. Mishurda and V. K. Vasudevan, "A Study of Phase Equilibria and Transformations in the Nb-Ti-Al System," *Symposium on New and Emerging Applications for Refractory Metals and Materials*, TMS, Rosemont, IL, Oct. (1998).

11. V. K. Vasudevan, "Progress in the Understanding of Phase Transformations in Gamma Titanium Aluminides," *International Symposium on Gamma Titanium Aluminides II*, San Diego, CA, Mar. 1-4, (1999).

12. D. M. Dimiduk and V. K. Vasudevan, "Isothermal and Continuous Cooling Decomposition of Alpha and Beta Phases in Gamma Titanium Aluminides," *Intern. Symp. on Gamma Titanium Aluminides II*, San Diego, CA, Mar. 1-4, (1999).

13. V. K. Vasudevan, "Phase Transformations in γ-TiAl Based Intermetallics," *University of Antwerp (RUCA), EMAT,* Antwerp, Belgium, June 11 (1999).

14. K. J. Leonard and V. K. Vasudevan, "Phase Transformaitons in Nb-Rich Nb-Ti-Al Alloys," *R. W. Cahn Symposium on Intermetallics for the Third Millenium*, ASMI/TMS, Cincinnati, OH, Oct./Nov. (1999).

15. J. C. Mishurda and V. K. Vasudevan, "The Use of Phase Equilibria in Microstructural Control of σ+γ and β+σ Alloys in the Nb-Ti-Al System," *Symposium on Refractory Metals and Alloys*, ASMI/TMS, Cincinnati, OH, Oct./Nov. (1999).

16. V. K. Vasudevan, "A Study of Phase Equilibria and Transformations in the Nb-Ti-Al System," *AFOSR Metallic Materials Contractors' Meeting, Materials Workshop,* San Diego, CA, Mar. 4-5 (1999).

17. K. J. Leonard and V. K. Vasudevan, "Site Occupancy Preferences in the B2 Ordered Solid Solution Phase of Nb-rich Nb-Ti-Al Alloys," *5th International Conference on Structural and Functional Intermetallics*, TMS, Vancouver, British Columbia, July (2000).

18. K. J. Leonard and V. K. Vasudevan, "Phase Equlibria at 1100°C in the Nb-Ti-Al System," *5th International Conference on Structural and Functional Intermetallics*, TMS, Vancouver, British Columbia, July (2000).

19. K. J. Leonard and V. K. Vasudevan, "The Observation of a New Tetragonal Phase in the Nb-Ti-Al System," *5th International Conference on Structural and Functional Intermetallics*, TMS, Vancouver, British Columbia, July (2000).

20. K. J. Leonard and V. K. Vasudevan, "The Observation of a New Tetragonal Phase in the Nb-Ti-Al System," *ASMI/TMS Fall Meeting*, St. Louis, MO, Oct. (2000).

8. PUBLICATIONS

(Includes those supported by the present award and by the companion AASERT award (F49620-95-1-0487)

Published

1. Jun Yang, "A Study of Phase Transformations and Microstructure Development in a Ti-22Al-26Nb Alloy," *M. S. Thesis*, University of Cincinnati, Cincinnati, OH, August (1996).

2. Narayanan Giridhar, "A Study of Phase Transformations and Microstructure Development in a 37Nb-37Ti-26Al Alloy," *M. S. Thesis*, University of Cincinnati, Cincinnati, OH, July (1997).

3. Bharath Natarajan, "The Effects of γ-Stabilizing Elements and Boron Additions on Microstructure Evolution in Gamma Titanium Aluminides," *M. S. Thesis*, University of Cincinnati, Cincinnati, OH, August (1997).

4. V. K. Vasudevan, J. Yang and A. P. Woodfield, "On the β to B2 Ordering Temperature in a Ti-22Al-26Nb Orthorhombic Titanium Aluminide," *Scripta Mater.*, **35**, pp. 1033-1039 (1996).

5. K. Madangopal, B. Natarajan, V. K. Vasudevan and D. M. Dimuduk, "Microstructure Evolution in Gamma Titanium Aluminides Containing Beta-Phase Stabilizers and Boron Additions," *in: Procs. of International Symposium on Structural Intermetallics II*, R. Darolia et al. (eds.), TMS, Warrendale, PA, pp. 235-244 (1997).

6. D. M. Dimiduk and V. K. Vasudevan, "Isothermal and Continuous Cooling Decomposition of Alpha and Beta Phases in Gamma Titanium Aluminides," *in: Gamma Titanium Aluminides II*, Y. W. Kim, D. M. Dimiduk and M. H. Loretto (eds.), TMS, Warrendale, PA, pp. 239-246 (1999).

7. K. J. Leonard, J. C. Mishurda, B. Molloseau, M. de Graef and V. K. Vasudevan, "Identification of a New Tetragonal Phase in the Nb-Ti-Al System," *Phil. Mag. Lett.* , **80(5)**, pp. 295-305 (2000).

8. K. J. Leonard, J. C. Mishurda and V. K. Vasudevan, "Examination of Solidification Pathways and the Liquidus Surface in the Nb-Ti-Al System," *Metall. Mater. Trans.*, in the press (2000).

9. K. J. Leonard and V. K. Vasudevan, "Phase Equilibria and Solid-State Transformations in Nb-Rich Nb-Ti-Al Intermetallic Alloys," *Intermetallics*, in the press (2000).

10. J. C. Mishurda and V. K. Vasudevan, "A Study of Phase Equilibria and Transformations in the Nb-Ti-Al System," *Intern. J. of Refractory Alloys and Hard Compounds*, accepted for publication (2000).

11. J. C. Mishurda and V. K. Vasudevan, "The Use of Phase Equilibria in Microstructural Control of $\sigma+\gamma$ and $\beta+\sigma$ Alloys in the Nb-Ti-Al System," *Intern. J. of Refractory Alloys and Hard Compounds* , accepted for publication (2000).

Submitted/Under Review

12. K. J. Leonard, J. C. Mishurda and V. K. Vasudevan, "Phase Equilibria at 1100°C in the Nb-Ti-Al System", *Mater. Sci. & Engrg.* (2000).

13. K. J. Leonard, N. Giridhar and V. K. Vasudevan, "Site Occupancy in the β_o/B2 Phase in Nb-Ti-Al Alloys," *Mater. Sci. Engrg.* (2000).

14. K. J. Leonard and V. K. Vasudevan, "Phase Transformations in a Nb-25Ti-25Al Alloy," *Acta Mater.* (2000).

15. K. J. Leonard, J. C. Mishurda and V. K. Vasudevan, "Decomposition of the β_o Phase to the ω-related, $P6_3/mcm$, hP18 Structure in Nb-(24-36)Ti-40Al Alloys," *Phil. Mag. A* (2000).

Articles Under Preparation

16. J. C. Mishurda and V. K. Vasudevan, "Phase Equilbria and Transformations in the Nb-Ti-Al System: $\beta+\sigma$ Alloys," *Acta Mater.*

17. J. C. Mishurda and V. K. Vasudevan, "An Estimate of the the Kinetics of the β_o to Orthorhombic Phase Transformation in the Nb-Ti-Al System, *Scripta Mater.*

18. K. J. Leonard, J. C. Mishurda and V. K. Vasudevan, "Phase Equilbria and Transformations in the Nb-Ti-Al System: $\sigma+\gamma$ Alloys," *Acta Mater.*

19. J. C. Mishurda, K. J. Leonard and V. K. Vasudevan, "Phase Equilbria and Transformations in the Nb-Ti-Al System: $\sigma+\delta$ Alloys," *Metall. Mater. Trans.*

20. J. C. Mishurda, K. J. Leonard and V. K. Vasudevan, "Phase Equilbria and Transformations in the Nb-Ti-Al System: $\beta+\delta$ Alloys," *Metall. Mater. Trans.*

21. K. J. Leonard, J. C. Mishurda, M. De Graef, D. Schryvers and V. K. Vasudevan, "High Resolution TEM Study of the New Tetragonal θ Phase in Nb-Ti-40Al Alloys, *Philos. Mag. A.*

22. V. K. Vasudevan and D. M. Dimiduk, "Phase Equilibria, Transformation Kinetics and Microstructure Evolution in Multicomponent Gamm Titanium Aluminides," *Acta Mater.*

23. K. Madangopal, B. Natarajan and V. K. Vasudevan, "Site Occupancy in the B2 Phase in Multicomponent γ-TiAl Alloys," *Scripta Mater.*

24. N. Giridhar and V. K. Vasudevan, "Decomposition of the β Phase in a 37Nb-37Ti-26Al Alloy," *Metall. Mater. Trans.*

25. J. Yang, K. J. Leonard and V. K. Vasudevan, "The B2 to O Transformation During Isothermal Aging in a Ti-22Al-27Nb Alloy," *Metall. Mater. Trans.*

26. V. K. Vasudevan, N. Giridhar and A. P. Woodfield, "On the Primary Orthorhombic Phase in a Ti-22Al-26Nb Alloy," *Metall. Mater. Trans.*

27. V. K. Vasudevan, D. Veeraraghavan and A. P. Woodfield, "The B2 to O Transformation During Continuous Cooling in a Ti-22Al-26Nb Alloy," *Metall. Mater. Trans..*

9. INTERACTIONS/TRANSITIONS

Several meetings have been held with Dr. Dennis Dimiduk of the Air Force Research Laboratory, and Drs. Madan Mendiratta and P. R. Subramanian of UES to discuss project directions, priorities, materials and processing, areas of mutual interest, collaborations and courses of action. The Nb-Ti-Al alloys studied were obtained from AFRL and collaborative work on these materials has been performed. The TiAl materials for the study were obtained from Drs. Dennis Dimiduk and Pat Martin (of Rockwell International Science Center). The work was conducted jointly with these persons. Joint presentations and publications have resulted and others are forthcoming.

10. HONORS/AWARDS

- *Fellow*, American Society for Materials International (2000).
- *Neil Wandmacher Outstanding Teaching Award*, College of Engineering, University of Cincinnati (2000).
- *Certificate of Recognition and Appreciation for Outstanding Service*, TMS (2000).
- *Fulbright Senior Scholar Award*, University of Antwerp (RUCA), EMAT, Antwerp, Belgium (1999).
- *Japan Society for the Promotion of Science Fellowship*, Kyoto University, Kyoto, Japan (1998).
- *Sigma Xi Young Investigator Award for Scientific Research*, University of Cincinnati (1997).
- *Certificate of Recognition and Appreciation for Outstanding Service*, TMS (1997).
- Nominated for the Univ. of Cinti. *A. B. (Dolly) Cohen Award for Excellence in Teaching* (1997).
- Elected to *Board of Review, Metallurgical and Materials Transactions*, (1996) - present.